MPeat2D – A fully coupled mechanical-ecohydrological model of peatland development in two dimensions

Adilan W. Mahdiyasa[1, 2], David J. Large[1], Matteo Icardi[3], Bagus P. Muljadi[1]

[1]Department of Chemical and Environmental Engineering, University of Nottingham, University Park, Nottingham NG7 2RD, UK
[2]Faculty of Mathematics and Natural Sciences, Bandung Institute of Technology, Bandung 40132, Indonesia
[3]School of Mathematical Sciences, University of Nottingham, University Park, Nottingham NG7 2RD, UK

Correspondence to: Adilan W. Mahdiyasa (adilan.widyawan@itb.ac.id)
                    David J. Large (david.large@nottingham.ac.uk)

Abstract. Higher dimensional models of peatland development are required to analyse the influence of spatial heterogeneity and complex feedback mechanisms. However, the current models exclude the mechanical process that leads to uncertainties in simulating the spatial variability of water table position, vegetation composition, and peat physical properties. Here, we propose MPeat2D, a peatland development model in two dimensions, which considers mechanical, ecological, and hydrological processes together with the essential feedback from spatial interactions. MPeat2D employs poroelasticity theory that couples fluid flow and solid deformation to model the influence of peat volume changes on peatland ecology and hydrology. To validate the poroelasticity formulation, the comparisons between numerical and analytical solutions of Mandel's problems for two-dimensional test cases are conducted. The application of MPeat2D is illustrated by simulating peatland growth over 5000 years above the flat and impermeable substrate with free-draining boundaries at the edges, using constant and variable climate. In both climatic scenarios, MPeat2D produces lateral variability of water table depth, which results in the variation of vegetation composition. Furthermore, the drop of the water table at the margin increases the compaction effect, leading to a higher value of bulk density and a lower value of active porosity and hydraulic conductivity. These spatial variations obtained from MPeat2D are consistent with the field observations, suggesting plausible outputs from the proposed model. By comparing the results of MPeat2D to a one-dimensional model and a two-dimensional model without the mechanical process, the significance of mechanical-ecohydrological feedback on spatial heterogeneity, peatland shape, carbon accumulation, and resilience is highlighted.

1 Introduction

In this paper, we provide a fully coupled mechanical-ecohydrological model of peatland development in two dimensions (2D). The continuum representation of the peatland employed by the proposed model results in the advancement of peatland modelling, particularly if we consider questions relating to the phenomena for which mechanical process and feedback are

essential components. Examples of these phenomena include the analysis of mechanical limits to peatland stability and the relationship between topography, peat physical properties, and carbon accumulation. The emphasis of this paper is to explain

35 the formulation of the model, which is developed from an earlier one-dimensional (1D) mechanical-ecohydrological models (Mahdiyasa et al., 2023; Mahdiyasa et al., 2022). Its application is illustrated through the simulations of the long-term peatland growth over millennia under idealised conditions. To consider the consequences of incorporating spatial variability and mechanical process on the peatland behaviour, we compare our results with the existing peatland growth models, including a 1D model without spatial variability MPeat (Mahdiyasa et al., 2023; Mahdiyasa et al., 2022) and a 2D stiff non-

40 continuum model DigiBog (Baird et al., 2012; Morris et al., 2012).

The spatial variability on the peatland is widely evidenced by the changes in the horizontal and vertical directions of peat physical properties, including bulk density, active porosity, and hydraulic conductivity. The horizontal variation of hydraulic conductivity was observed by Lapen et al. (2005), who found that hydraulic conductivity is lower at the margin than at the centre based on the field measurements and analysis of the peatland groundwater flow model. Field observations from Baird

45 et al. (2008) and Lewis et al. (2012), who measured lateral variability of the hydraulic conductivity in a raised and a blanket peatland, respectively, agree with the Lapen et al. (2005) finding. Lewis et al. (2012) also observed the lateral variability in bulk density, which increased from the centre toward the margin. In the vertical direction, deeper peat exhibits a higher value of bulk density and a lower value of active porosity and hydraulic conductivity, with abrupt changes occurring between the unsaturated and saturated zones (Clymo, 2004, 1984; Hoag and Price, 1997; Hoag and Price, 1995; Quinton et al., 2008;

50 Quinton et al., 2000; Fraser et al., 2001).

The spatial variations of peat physical properties occur because of the fully coupled mechanical-ecohydrological processes. As a porous medium with a low value of Young's modulus (Long, 2005; Mesri and Ajlouni, 2007; Boylan et al., 2008; Dykes and Warburton, 2008), the peat body is susceptible to deformation. The deformation is non-uniform throughout the peatland area due to the spatial variations of water table depth that influence the effective stress (Whittington and Price,

55 2006; Price, 2003; Price et al., 2005; Waddington et al., 2010). For example, the increase in water table depth at the margin leads to higher bulk density and lower active porosity and hydraulic conductivity, preventing greater water discharge from the deeper peat. Consequently, Lapen et al. (2005) posited that a lower hydraulic conductivity at the margin has a significant influence on maintaining the wet condition at the centre, which in turn affects peat accumulation. Therefore, the spatial variations of peat physical properties potentially provide essential feedback as the peatland develops.

60 Higher dimensional models of peatland development assume constant or limited spatial variations of peat physical properties and ignore mechanical feedback (e.g., Ingram, 1982; Winston, 1994; Armstrong, 1995; Korhola et al., 1996; Borren and Bleuten, 2006; Baird et al., 2012; Morris et al., 2012; Swinnen et al., 2019). For example, Borren and Bleuten (2006) proposed a three-dimensional model (3D) of peatland development based on the groundwater flow model (Boussinesq, 1871) and focused on the ecohydrological feedback between water table position with peat production and decomposition

65 following the Clymo (1984) model. The mechanical compaction is assumed to be negligible, and the spatial variations in the bulk density and hydraulic conductivity are obtained based on the empirical relationship between different peatland types,

consisting of bog, throughflow fen, and fen. DigiBog (Baird et al., 2012; Morris et al., 2012) is a 1D, 2D, or 3D model of peatland development that accommodates the spatial changes in hydraulic conductivity through the differences in remaining mass that are affected by water table position and decomposition processes (Moore et al., 2005; Quinton et al., 2000).

70 Although DigiBog captures more complex feedback between ecological and hydrological processes than the model from Borren and Bleuten (2006), the omission of mechanical feedback leads to the assumption of constant active porosity and bulk density as the peatland grows. Cobb et al. (2017) developed a 2D tropical peatland growth model to analyse the influence of climate, particularly the rainfall pattern, on carbon storage. This model simulates the dynamics of the water table and peat accumulation through the groundwater flow model (Boussinesq, 1871) and the difference between peat

75 production and decomposition. The carbon storage is estimated from the stable peat surface Laplacian that is affected by the rate of peat production and decomposition. The peat surface Laplacian indicates the curvature of the peat surface, calculated as the sum of second derivatives of surface elevation. Although surface Laplacian provides information related to the peatland morphology, this model ignores the mechanical feedback and assumes a constant value of hydraulic conductivity that becomes the source of uncertainty in estimating the peatland carbon storage.

80 This paper, therefore, sets out to (1) provide the formulation of a fully coupled mechanical-ecohydrological model of peatland development in 2D called MPeat2D, (2) investigate model outputs in the idealised peatland growth scenario, (3) analyse the potential consequences of mechanical-ecohydrological feedback on the long-term peatland carbon accumulation and resilience by comparison with the other peatland development models. The structure of this paper is presented in three main parts. First, we consider the mathematical formulation, consisting of mechanical, ecological, and hydrological

85 submodels, together with the numerical verification of the MPeat2D. Second, we explain how to implement MPeat2D to simulate long-term peatland growth over millennia and provide examples of model outputs. Third, we examine the implications obtained from MPeat2D to understand peatland behaviour and conclude the analysis by addressing the areas in which further development from the model is required. Although MPeat2D is focused on ombrotrophic peatlands with temperate climates, the framework proposed in this paper could be employed to model the other peatland types.

2 Model formulation and verification

90 MPeat2D is a fully coupled mechanical, ecological, and hydrological model of long-term peatland growth in two dimensions, which takes spatial variability and structure into consideration. MPeat2D is developed based on the continuum concept (Irgens, 2008; Jog, 2015) that assumes peatland constituents, both solid and fluid particles, entirely fill the peatland body. Through this approach, the conservation of mass can be appropriately defined to formulate mechanical processes on

95 the peatland obtained from the coupling between solid deformation and fluid flow or known as poroelasticity that becomes the core of the model (see the mechanical submodel) (Biot, 1941; Detournay and Cheng, 1993; De Boer, 2000; Wang, 2000; Coussy, 2004). The mechanical deformation of peat pores space affects physical properties, including bulk density, active porosity, and hydraulic conductivity, resulting in different peatland behaviour (Fig. 1). For example, the changes in active

porosity and hydraulic conductivity influence the water table position, which in turn determines peat production and
100 decomposition processes (Belyea and Clymo, 2001; Clymo, 1984). Furthermore, the proportion of plant functional types
(PFT) and the plant weight are also affected because they are a function of the water table depth (Moore et al., 2002; Munir
et al., 2015; Peltoniemi et al., 2016; Kokkonen et al., 2019; Laine et al., 2021). The plant weight at the top surface produces
loading that leads to compaction and provides feedback on the peat physical properties. By having fully coupled mechanical,
ecological, and hydrological processes, MPeat2D incorporates realistic spatial variability on the peatland and allows for
105 more significant insights into the interplay between these complex feedback mechanisms. As explained below, the
formulation of MPeat2D is divided into mechanical, ecological, and hydrological submodels.
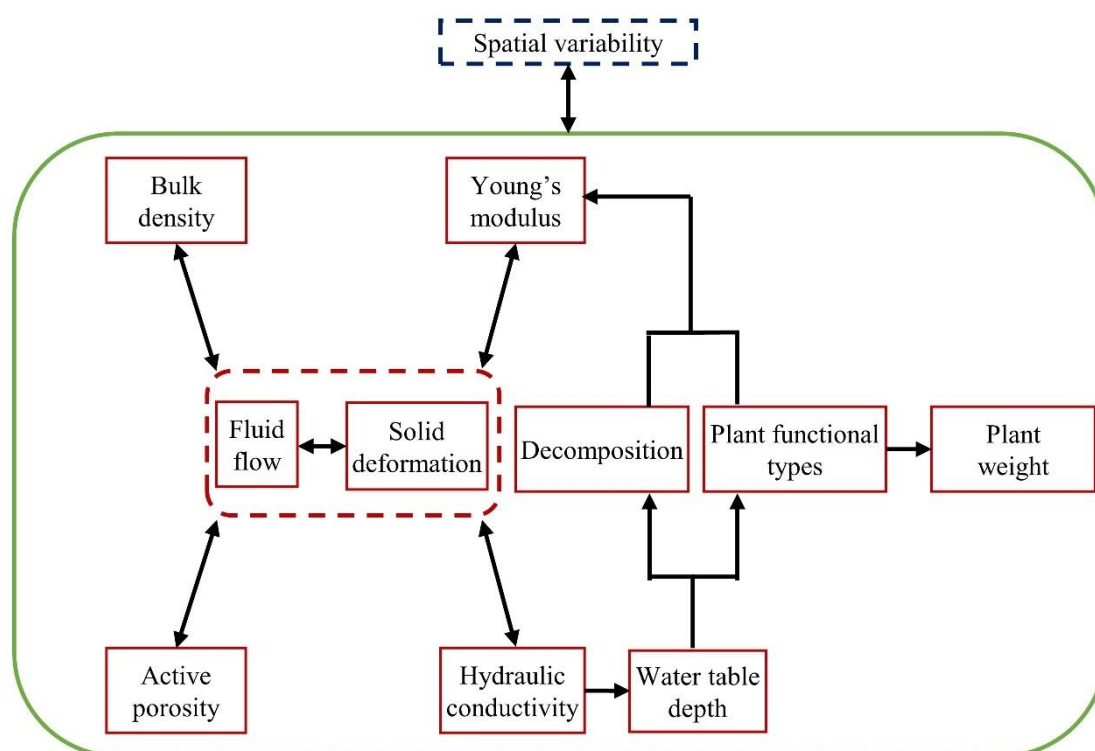
Figure 1: Illustrative formulation of MPeat2D that involves mechanical, ecological, and hydrological processes together with the feedback from spatial variability on the peatland under a single mathematical and numerical framework.

2.1 Mechanical submodel

The mechanical deformation on the peat body is influenced by the stiffness of the peat solid skeleton and the behaviour of
the pore fluid. Reeve et al. (2013) found that a higher value of Young's modulus, which represents the stiffness of the
material, leads to a lower deformation effect on the peat body. Furthermore, the characteristics of fluid contained in the peat
pore space, including gas content and degree of saturation, also significantly affect the deformation due to the presence of

115   pore fluid pressure (Boylan et al., 2008; Price and Schlotzhauer, 1999; Price, 2003). Therefore, the mechanical submodel is developed based on the poroelasticity theory, which couples solid deformation and fluid flow.

We employ a fully saturated poroelasticity in 2D (Biot, 1941) to model the saturated zone of the peatland below the water table, with the governing equations as follows. The equation of equilibrium can be formulated by considering the stress tensor acting on a small elementary area, as written below

120   $$\overline{\nabla}^{\mathrm{T}}\boldsymbol{\sigma} + \mathbf{b} = 0, \tag{1}$$

with $\overline{\nabla} = \begin{bmatrix} \frac{\partial}{\partial x} & 0 \\ 0 & \frac{\partial}{\partial y} \\ \frac{\partial}{\partial y} & \frac{\partial}{\partial x} \end{bmatrix}$ and $\mathbf{b} = \begin{bmatrix} 0 & (\rho_w\phi + \rho(1-\phi))g \end{bmatrix}^{\mathrm{T}}$. In this formulation $\boldsymbol{\sigma} = \begin{bmatrix} \sigma_{xx}, \sigma_{yy}, \sigma_{xy} \end{bmatrix}^{\mathrm{T}}$ is the total stress tensor

(Pa), $\mathbf{b}$ is the body force (N m^{-3}), ρ_w is the water density (kg m^{-3}), ρ is the peat bulk density (kg m^{-3}), ϕ is the active porosity (–) and g is the acceleration of gravity (m s^{-2}). The presentation in terms of matrix form provides convenient notation for the derivation of weak form and numerical calculation (Jha and Juanes, 2014).

125   The stresses on the peat body are distributed to the solid skeleton and pore fluid, resulting in solid displacement and pore fluid pressure. The stress associated with solid displacement is known as effective stress, and it is defined as

$$\boldsymbol{\sigma}' = \boldsymbol{\sigma} - \alpha\mathbf{m}p, \tag{2}$$

where $\boldsymbol{\sigma}' = \begin{bmatrix} \sigma'_{xx}, \sigma'_{yy}, \sigma'_{xy} \end{bmatrix}^{\mathrm{T}}$ is the effective stress tensor (Pa), $\boldsymbol{\sigma} = \begin{bmatrix} \sigma_{xx}, \sigma_{yy}, \sigma_{xy} \end{bmatrix}^{\mathrm{T}}$ is the total stress tensor (Pa), α is the Biot's coefficient, $\mathbf{m} = \begin{bmatrix} 1 & 1 & 0 \end{bmatrix}^{\mathrm{T}}$ is the vector form of Kronecker's delta, and p is the pore water pressure (Pa). The

130   linear constitutive law gives the relation between effective stress tensor and strain tensor through the following equation

$$\boldsymbol{\sigma}' = \mathbf{D}\boldsymbol{\epsilon}, \tag{3}$$

with $\mathbf{D} = \frac{E}{(1+\nu)(1-2\nu)}\begin{bmatrix} 1-\nu & \nu & 0 \\ \nu & 1-\nu & 0 \\ 0 & 0 & \frac{1-2\nu}{2} \end{bmatrix}$. In this formulation $\boldsymbol{\sigma}' = \begin{bmatrix} \sigma'_{xx}, \sigma'_{yy}, \sigma'_{xy} \end{bmatrix}^{\mathrm{T}}$ is the effective stress tensor (Pa),

E is the Young's modulus (Pa), ν is the Poisson's ratio (−), and $\boldsymbol{\epsilon} = \begin{bmatrix} \epsilon_{xx}, \epsilon_{yy}, \epsilon_{xy} \end{bmatrix}^{\mathrm{T}}$ is the strain tensor (−). The relation between strain tensor and displacement is provided by the kinematics relations reads

135   $$\boldsymbol{\epsilon} = \overline{\nabla}\mathbf{u}, \tag{4}$$

where $\boldsymbol{\epsilon} = \begin{bmatrix} \epsilon_{xx}, \epsilon_{yy}, \epsilon_{xy} \end{bmatrix}^{\mathrm{T}}$ is the strain tensor (−) and $\mathbf{u} = \begin{bmatrix} u_x, u_y \end{bmatrix}^{\mathrm{T}}$ is the displacement (m). Finally, to complete the governing equations of the mechanical submodel, we employ the conservation of mass for solid and fluid constituents. By assuming that water flow in the peat pore space follows Darcy's law and the volumetric strain is the sum of linear strains, we can formulate the relation between solid deformation, pore water pressure, and the water flow in the peat pore space as

140 $$\alpha \frac{\partial \epsilon}{\partial t} + S_S \frac{\partial p}{\partial t} = \nabla \cdot (\kappa \nabla p),$$ (5)

where α is the Biot's coefficient $(-)$, $\epsilon = \epsilon_{xx} + \epsilon_{yy}$ is the volumetric strain $(-)$, S_s is the specific storage (m^{-1}), p is the pore water pressure (Pa), and κ is the hydraulic conductivity (m s^{-1}).

In the unsaturated zone above the water table, we assume that the air pressure is equal to the atmospheric pressure because the water table depth is usually less than 0.5 m in the peatland (Ballard et al., 2011; Swinnen et al., 2019; Mahdiyasa et al.,

145 2022). Consequently, we can expand Eq. (5) to model the unsaturated zone by introducing parameters α_w and M_w that depend on the degree of saturation of water as follows (Cheng, 2020)

$$\alpha_w \frac{\partial \epsilon}{\partial t} + \frac{1}{M_w} \frac{\partial p}{\partial t} = \nabla \cdot (\kappa \nabla p),$$ (6)

with $\alpha_w = S_w$ and $M_w = \frac{\gamma_w(1-\lambda)}{\phi \lambda \mu} S_w^{-1/\lambda} \left(1 - S_w^{1/\lambda}\right)^{\lambda}$. In this formulation $\epsilon = \epsilon_{xx} + \epsilon_{yy}$ is the volumetric strain $(-)$, p is the pore water pressure (Pa), κ is the hydraulic conductivity (m s^{-1}), S_w is the degree of saturation of water $(-)$, γ_w is the

150 specific weight of water (N m^3), ϕ is the active porosity $(-)$, λ is the first water retention empirical constant $(-)$, and μ is the second water retention empirical constant (m^{-1}).

The discretisation is required in order to solve the partial differential equations from poroelasticity formulation. In 1D, the discretisation is relatively simple because it is conducted over a vertically oriented domain, the length of which represents the height of a peatland (Mahdiyasa et al., 2023; Mahdiyasa et al., 2022). However, in 2D, the discretisation becomes more

155 complex and is carefully done to circumvent numerical instabilities (George, 2000; Edelsbrunner, 2001; Zhu et al., 2006). We implement the Delaunay triangulation, which provides an optimal and non-overlapping connection between the neighbouring triangles from the data sets of points to create a 2D mesh (Shewchuk, 2002). The Delaunay triangulation does not require a predetermined equation for domain descriptions, which is relevant for our model because the internal and external feedback mechanisms influence the shape and domain of the peatland during the development process.

160 The peat stiffness, represented by Young's modulus, is modelled as a function of decomposition (Zhu et al., 2020) and plant functional types (PFT) (Whittington et al., 2007), following the formulation from Mahdiyasa et al. (2023)

$$E = \chi \left(1 + \theta_t^{\zeta}\right)(b_1 c_1 + b_2 c_2 + b_3 c_3),$$ (7)

where E is the Young's modulus (Pa), χ is the first Young's modulus parameter (Pa), ζ is the second Young's modulus parameter $(-)$, θ is the remaining mass $(-)$, b_1, b_2, b_3 are the coefficient to couple PFT with Young's modulus $(-)$, and

165 c_1, c_2, c_3 are the PFT proportions $(-)$ with the indices $1, 2, 3$ indicating shrub, sedge, and *Sphagnum*, respectively. The interactions between peat stiffness and the load from plant weight, new layer addition, and body force determine the vertical and horizontal displacement of peat solid particles, which affects the bulk density and active porosity due to the changes in the peat volume. We proposed the influence of solid displacement on the peat bulk density and active porosity in 2D as follows

$$\rho_t = \frac{\rho_{t-1}}{1+\beta_\rho \nabla \cdot \mathbf{u}}, \tag{8}$$

$$\phi_t = \frac{\phi_{t-1}+\beta_\phi \nabla \cdot \mathbf{u}}{1+\nabla \cdot \mathbf{u}}, \tag{9}$$

where ρ is the bulk density (kg m^{-3}), β_ρ is the bulk density parameter ($-$), ϕ is the active porosity ($-$), β_ϕ is the active porosity parameter ($-$), and $\mathbf{u} = \left[u_x, u_y\right]^{\mathrm{T}}$ is the displacement (m).

2.2 Ecological submodel

We use the formulation from Morris et al. (2015) for the peat production model that is influenced by the water table depth and air temperature, written as

$$\psi = 0.001(9.3 + 133z - 0.022(100z)^2)^2(0.1575Temp + 0.0091), \text{ for } 0 \le z \le 0.668 \tag{10}$$

$$\psi = 0, \text{ for } z > 0.668,$$

where ψ is the peat production (kg m^{-2} yr^{-1}), z is the water table depth (m), and $Temp$ is the air temperature (°C). Peat production and the PFT proportion are employed to model the plant weight at the top surface through the following equation (Mahdiyasa et al., 2023; Mahdiyasa et al., 2022; Moore et al., 2002)

$$Y = c_1 \left(10^{\frac{log_{10}(\psi)+0.409}{0.985}}\right)(1 + d_1)g + c_2\left(10^{log_{10}(\psi)+0.001}\right)(1 + d_2)g + (c_3 0.144)(1 + d_3)g, \tag{11}$$

where Y is the plant weight (Pa), ψ is the peat production (kg m^{-2} yr^{-1}), g is the acceleration of gravity (m s^{-2}), c_1, c_2, c_3 are the PFT proportions ($-$), and d_1, d_2, d_3 are the constants for plant wet condition ($-$) with the indices $1, 2, 3$ indicating shrub, sedge, and *Sphagnum*, respectively. The proportions of PFT vary depending on the position of the water table, with the shrub becoming the dominant PFT in the low water table condition (Moore et al., 2002; Potvin et al., 2015; Kettridge et al., 2015). Therefore, we use a linear regression model from Mahdiyasa et al. (2023), which was developed from Moore et al. (2002) data, to model the relationship between PFT proportions with the water table

$$c_1 = 2.23z - 0.28, \tag{12}$$

$$c_2 = -1.42z + 0.63, \tag{13}$$

$$c_3 = -0.81z + 0.64, \tag{14}$$

where c_1, c_2, c_3 are the PFT proportions ($-$) with the indices $1, 2, 3$ indicating shrub, sedge, and *Sphagnum*, respectively, and z is the water table depth (m). We assign the minimum value of each PFT proportion equal to zero if the value is negative and normalise the total proportion.

The decomposition processes occur in the saturated and unsaturated zones of the peatland at different rates. In the saturated zone below the water table, the rate of decay is low due to the anaerobic condition, while in the unsaturated zone above the

water table, the rate of decay is significantly higher as a consequence of the aerobic condition that supports the decomposition processes. We follow the model from Clymo (1984) to calculate the changes in peat mass due to the decomposition

200
$$\frac{dm}{dt} = -\eta m,$$
(15)

where m is the mass per unit area (kg m^{-2}) and η is the rate of decay (yr^{-1}). The effect of decomposition is represented as the remaining mass, which is defined as the ratio between mass at time t, which has experienced decay, and the initial mass (Mahdiyasa et al., 2022; Baird et al., 2012; Morris et al., 2012; Morris et al., 2015)

$$\theta_t = \frac{m_t}{m_0},$$
(16)

205 where θ is the remaining mass (−), m_t is the mass per unit area at time t (kg m^{-2}), and m_0 is the initial mass per unit area (kg m^{-2}).

2.3 Hydrological submodel

We model the peatland groundwater flows in 2D using the Boussinesq equation (Boussinesq, 1871) subject to net rainfall that acts as a source term (Cobb et al., 2017; Baird et al., 2012; Morris et al., 2012)

210
$$S_s \frac{\partial \Gamma}{\partial t} = \nabla \cdot (\kappa \nabla \Gamma) + r,$$
(17)

where Γ is the water table height (m), S_s is the specific storage (m^{-1}), κ is the hydraulic conductivity (m s^{-1}), and r is the net rainfall (m yr^{-1}) that is defined as precipitation minus evapotranspiration. Boussinesq equation is developed based on the Dupuit and Forchheimer (D-F) assumption (Dupuit, 1863; Forchheimer, 1930), which states that groundwater flows horizontally in unconfined aquifers. The D-F assumption is appropriate to model the peatland groundwater because the

215 peatland lateral distance is much wider than the thickness, which leads to the dominant horizontal flow. We assume that the height of the water table cannot surpass the height of the peatland because the water will flow as surface water (Mahdiyasa et al., 2022; Morris et al., 2011). Consequently, the water table depth is obtained from the difference between peatland height and water table height as follows

$$z = h - \Gamma,$$
(18)

220 where z is the water table depth (m), h is the peatland height (m), and Γ is the water table height (m).

The mechanical deformation changes the peat pore structure, leading to variations in the active porosity (Eq. (9)) and influencing water flow through the pore space. Therefore, we implement the hydraulic conductivity model from Mahdiyasa et al. (2022), who formulate the changes in hydraulic conductivity as a function of active porosity

$$\kappa_t = \kappa_0 \left(\frac{\phi_t}{\phi_0}\right)^{\xi},$$ (19)

225 where κ is the hydraulic conductivity (m s^{-1}), κ_0 is the initial value of hydraulic conductivity (m s^{-1}), ϕ is the active porosity $(-)$, ϕ_0 is the initial value of active porosity $(-)$, and ξ is the hydraulic conductivity parameter $(-)$. Through this approach, we can capture the effect of mechanical deformation on the peatland hydrology.

2.4 Numerical verification

The verification is focused on the mechanical submodel, particularly the poroelasticity formulation, by comparing numerical

230 calculations with analytical solutions from Mandel's problem (Mandel, 1953). Uniform vertical load $2F$ is applied to a rectangular sample through a rigid and frictionless plate of width $2a$ and height $2H$, with drainage to the two sides in lateral condition as shown in Fig. 2. The deformation of the sample is forced to be in-plane strain condition by preventing all deformation in the direction perpendicular to the plane. The pore water pressure distribution will be homogeneous at the instant loading, but when drainage starts, the pore water pressure at two sides, $x = -a$ and $x = a$, are reduced to zero and

235 followed by the pore water pressure in the interior. Because the discharge has only a horizontal component, the pore water pressure, stress, and strain are independent of the y-coordinate. Furthermore, $\sigma_{xx} = 0$, $\sigma_{xy} = 0$, u_x is independent of y, and u_y is independent of x. Since the problem is symmetric, we solve only the upper right quadrant of the xy plane. We use 441 nodes and 800 elements to generate the simulations. The data for analytical and numerical solutions of this problem are stated in Table 1.

240 The analytical solutions to Mandel's problem for the pore water pressure, horizontal, and vertical displacement are (Cheng and Detournay, 1988; Abousleiman et al., 1996; Phillips and Wheeler, 2007)

$$p = \frac{2FB(1+\nu_u)}{3a} \sum_{i=1}^{\infty} \frac{\sin \omega_i}{\omega_i - \sin \omega_i \cos \omega_i} \left(\cos \frac{\omega_i x}{a} - \cos \omega_i\right) \exp\left(-\frac{\omega_i^2 c_\nu t}{a^2}\right),$$ (20)

$$u_x = \left[\frac{F\nu}{2Ga} - \frac{F\nu_u}{Ga} \sum_{i=1}^{\infty} \frac{\sin \omega_i \cos \omega_i}{\omega_i - \sin \omega_i \cos \omega_i} \exp\left(-\frac{\omega_i^2 c_\nu t}{a^2}\right)\right] x + \frac{F}{G} \sum_{i=1}^{\infty} \frac{\cos \omega_i}{\omega_i - \sin \omega_i \cos \omega_i} \sin \frac{\omega_i x}{a} \exp\left(-\frac{\omega_i^2 c_\nu t}{a^2}\right),$$ (21)

$$u_y = \left[-\frac{F(1-\nu)}{2Ga} + \frac{F(1-\nu_u)}{Ga} \sum_{i=1}^{\infty} \frac{\sin \omega_i \cos \omega_i}{\omega_i - \sin \omega_i \cos \omega_i} \exp\left(-\frac{\omega_i^2 c_\nu t}{a^2}\right)\right] y,$$ (22)

245 with $\tan \omega_i = \frac{1-\nu}{\nu_u - \nu} \omega_i$. In this analytical solutions p is the pore water pressure (Pa), u_x is the horizontal displacement (m), u_y is the vertical displacement (m), F is the force (N), B is the Skempton's coefficient $(-)$, G is the shear modulus (Pa), ν is the Poisson's ratio $(-)$, and ν_u is the undrained Poisson's ratio $(-)$.
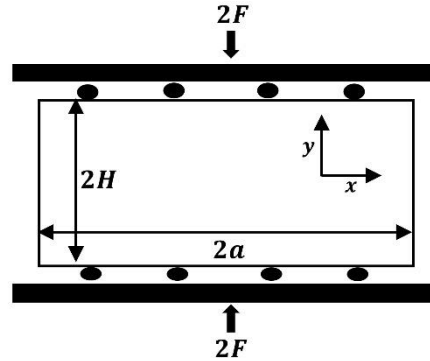
Figure 2: The illustration of Mandel's problem for the two-dimensional poroelasticity verification.

Table 1: Input data for numerical and analytical solutions of Mandel's problem.

Name	Symbol	Value	Unit
Horizontal and vertical distance	a	1	m
Consolidation coefficient	c_v	0.17	$\mathrm{m^2\,s^{-1}}$
Force	F	2×10^4	N
Initial value of pore water pressure	p_0	1×10^4	Pa
Porosity	ϕ	0.375	−
Poisson's ratio	ν	0.2	−
Undrained Poisson's ratio	ν_u	0.5	−
Hydraulic conductivity	κ	1×10^{-5}	$\mathrm{m\,s^{-1}}$
Specific storage	S_s	3.5×10^{-10}	$\mathrm{m^{-1}}$
Bulk modulus	K	1.2×10^8	Pa
Skempton's coefficient	B	0.95	−
Shear modulus	G	4×10^7	Pa

The comparison between numerical and analytical solutions for Mandel's problem for normalised pore water pressure, normalised horizontal displacement, and normalised vertical displacement are shown in Fig. 3 at various dimensionless time $t^* = c_v t/a^2$. The mean absolute errors for normalised pore water pressure and displacement are small. The first variable, normalised pore water pressure, has a mean absolute error of around 3.8×10^{-3}, 3.7×10^{-4}, and 5.2×10^{-6} at dimensionless time equal to 0.01, 0.1, and 0.5, respectively. For the second variable, normalised horizontal displacement, has a mean absolute error of around 2.8×10^{-3} and 1.4×10^{-6} at dimensionless time equal to 0.1 and 0.5, respectively. Finally, the mean absolute error of normalised vertical displacement is about 1.1×10^{-3} at dimensionless time equal to 0.1 and 5.8×10^{-7} at dimensionless time equal to 0.5.

Mandel's problem has an interesting characteristic related to the behaviour of pore water pressure. In the centre of the sample, the pore water pressure will be higher than the initial pressure for a small time interval. The value of normalised pore water pressure is greater than one at $t^* = 0.01$ and $t^* = 0.1$ (Fig. 3a). This phenomenon is denoted as the Mandel-

Cryer effect, and it occurs due to the deformation and rigid plate conditions producing an additional source term for the pore
265   water pressure distribution (Phillips and Wheeler, 2007; Duijn and Mikelic, 2021).
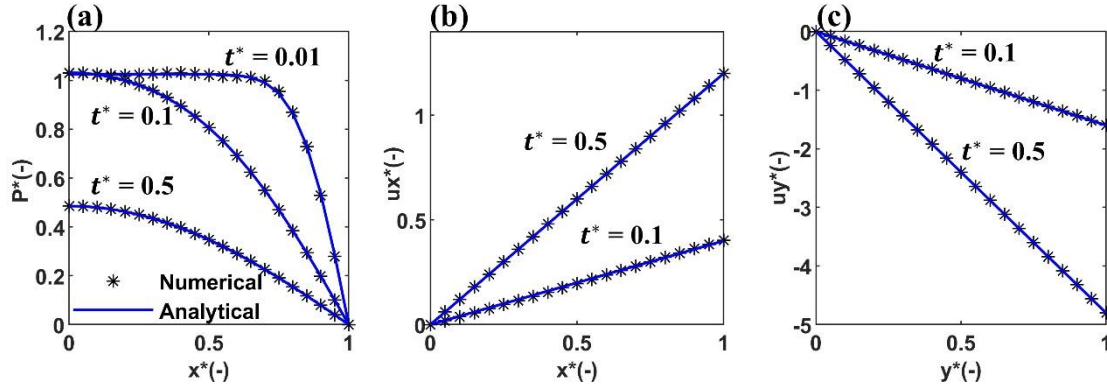
Figure 3: Numerical and analytical solutions of Mandel's problem at various dimensionless time $t^* = c_v t / a^2$ **for (a) normalised pore water pressure** $P^* = \frac{p}{p_0}$, **(b) normalised horizontal displacement** $u_x^* = \frac{u_x}{u_{x0}}$, **and (c) normalised vertical displacement** $u_y^* = \frac{u_y}{u_{y0}}$. **The initial displacements in the horizontal and vertical directions are obtained from** $u_{x0} = \frac{Fv_u x}{2Ga}$ **and** $u_{y0} = \frac{F(1-v_u)y}{2Ga}$, **respectively. In**
270   **this verification,** $x^* = \frac{x}{a}$ **is the normalised horizontal distance and** $y^* = \frac{y}{a}$ **is the normalised vertical distance.**

3 Model implementation

We simulate long-term peatland development over 5000 years with flat, impermeable, and rigid substrates, constrained by the parallel rivers at the edges (Ingram, 1982), with the parameter values summarised in Table 2. We assume the rivers do not incise, which could affect the water discharge (Glaser et al., 2004). Therefore, we implement no displacement and no
275   flux boundary conditions at the bottom and zero pore water pressure at the edges. To reduce the computational time, we model half of the peatland domain from the central vertical axis to the one river with a distance of 500 m due to the symmetric growth assumption of the peatland (Baird et al., 2012; Morris et al., 2012). The boundary conditions for the central axis are impermeable without experiencing horizontal displacement.

The total load on this system is associated with the surficial peat addition (Eq. (10)), plant weight (Eq. (11)), and body force
280   (Eq. (1)). The surficial peat addition and plant weight are applied at the surface, while the body force acts throughout the peatland area. The surface loadings are influenced by the peat production and vegetation composition consisting of shrub, sedge, and *Sphagnum*. Different from the surface loadings that are controlled by external sources, the body force is obtained from peatland self-weight, which is determined by the peat bulk density, water density, and active porosity.

To illustrate how MPeat2D works, we run two groups of simulations based on the climatic influence. In the first group, we
285   employ constant net rainfall (0.8 m yr^{-1}) and air temperature (6 °C) to provide the basic simulation related to the influence of mechanical-ecohydrological feedback and spatial heterogeneity of peat physical properties, water table depth, PFT proportion, and plant weight on peatland behaviour (Fig. 4). In the second group, we use a non-constant annual time series of

net rainfall and air temperature generated from sinusoidal function with some noise (Mahdiyasa et al., 2023; Mahdiyasa et al., 2022), with the range value of $0.6 - 1 \, \text{m} \, \text{yr}^{-1}$ and $4 - 7\,°C$, respectively (Morris et al., 2015; Young et al., 2021;

290   Young et al., 2019). The fluctuations of wet and dry conditions from climate input in the second group are developed to analyse the peatland response to the changing climate during the long-term development process.

Table 2: Parameter default values for the simulations.

Name	Symbol	Value	Unit	Reference
Unsaturated zone decay rate	η_{un}	5×10^{-2}	yr^{-1}	Clymo (1984)
Saturated zone decay rate	η_{sa}	8×10^{-5}	yr^{-1}	Clymo (1984)
Biot's coefficient	α	1	$-$	Terzaghi (1943)
Poisson's ratio	ν	0.2	$-$	Present study
Bulk density initial value	ρ_0	50	$\text{kg} \, \text{m}^{-3}$	Lewis et al. (2012)
Bulk density parameter	β_ρ	3	$-$	Present study
Active porosity initial value	ϕ_0	0.8	$-$	Quinton et al. (2000)
Active porosity parameter	β_ϕ	2	$-$	Present study
Hydraulic conductivity initial value	κ_0	1×10^{-2}	$\text{m} \, \text{s}^{-1}$	Hoag and Price (1995)
Hydraulic conductivity parameter	ξ	15	$-$	Mahdiyasa et al. (2022)
Degree of saturation of water	S_w	0.4	$-$	Mahdiyasa et al. (2022)
Water retention empirical constant 1	λ	0.5	$-$	Mahdiyasa et al. (2022)
Water retention empirical constant 2	μ	0.4	m^{-1}	Mahdiyasa et al. (2022)
Specific storage	S_s	1.4×10^{-2}	m^{-1}	Hogan et al. (2006)
Young's modulus parameter 1	χ	4×10^5	Pa	Present study
Young's modulus parameter 2	ζ	0.1	$-$	Mahdiyasa et al. (2022)
Shrub-Young's modulus parameter	b_1	1.25	$-$	Mahdiyasa et al. (2023)
Sedge-Young's modulus parameter	b_2	1	$-$	Mahdiyasa et al. (2023)
Sphagnum-Young's modulus parameter	b_3	0.75	$-$	Mahdiyasa et al. (2023)
Shrub constant	d_1	0.4	$-$	Mahdiyasa et al. (2022)
Sedge constant	d_2	0.4	$-$	Mahdiyasa et al. (2022)
Sphagnum constant	d_3	20	$-$	Mcneil and Waddington (2003)

295
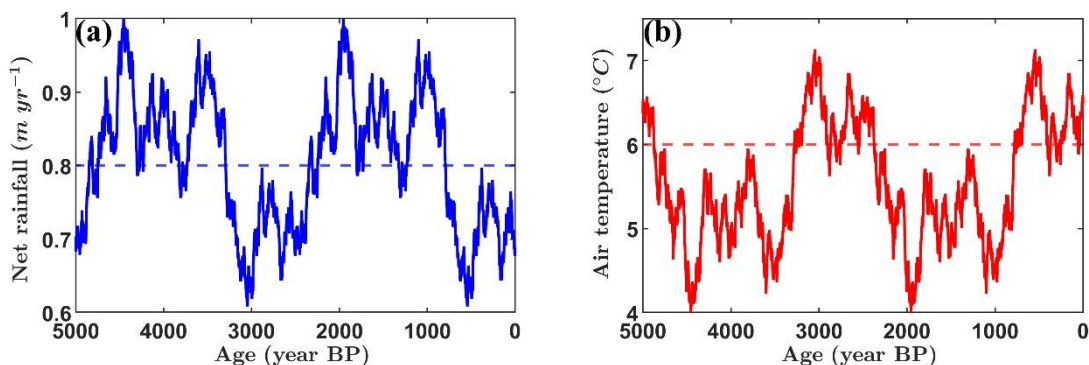
Figure 4: The climate profile for (a) net rainfall and (b) air temperature over 5000 years under constant and non-constant conditions. The values of constant climate are $0.8\,\text{m}\,\text{yr}^{-1}$ and $6\,°\text{C}$ indicated by dashed lines, while the non-constant climate specified by continuous lines fluctuating between $0.6 - 1\,\text{m}\,\text{yr}^{-1}$ and $4 - 7\,°\text{C}$ for net rainfall and air temperature, respectively.

We compare the results obtained from MPeat2D with the previously developed mechanical-ecohydrological model of peatland development in 1D called MPeat (Mahdiyasa et al., 2022; Mahdiyasa et al., 2023) to assess feedbacks or other physical phenomena that might be unresolved by the latter. The comparison is conducted for the water table depth, peatland height, and cumulative carbon from the centre area using the same parameters and climatic influence summarised in Table 2 and Fig. 4, respectively. In both models, cumulative carbon is obtained from cumulative mass multiplied by 47% of the carbon content (Loisel et al., 2014).

4 Simulation results

4.1 First group: Constant climate

In the initial stage of development, the peatland shape is relatively flat, with a low value of bulk density and a high value of active porosity and hydraulic conductivity. By 5000 years, a dome-shaped peatland is produced with the maximum thickness obtained at the centre and decreases toward the margin. The increasing thickness leads to higher loading and a more significant deformation effect on the peat pore structure, which affects the peat physical properties. The changes in peat physical properties during the development process exhibit spatial variabilities in the vertical and horizontal directions with the range value between $50 - 100\,\text{kg}\,\text{m}^3$, $0.49 - 0.8$, and $5.5 \times 10^{-6} - 1 \times 10^{-2}\,\text{m}\,\text{s}^{-1}$ for bulk density, active porosity, and hydraulic conductivity, respectively (Fig. 5).
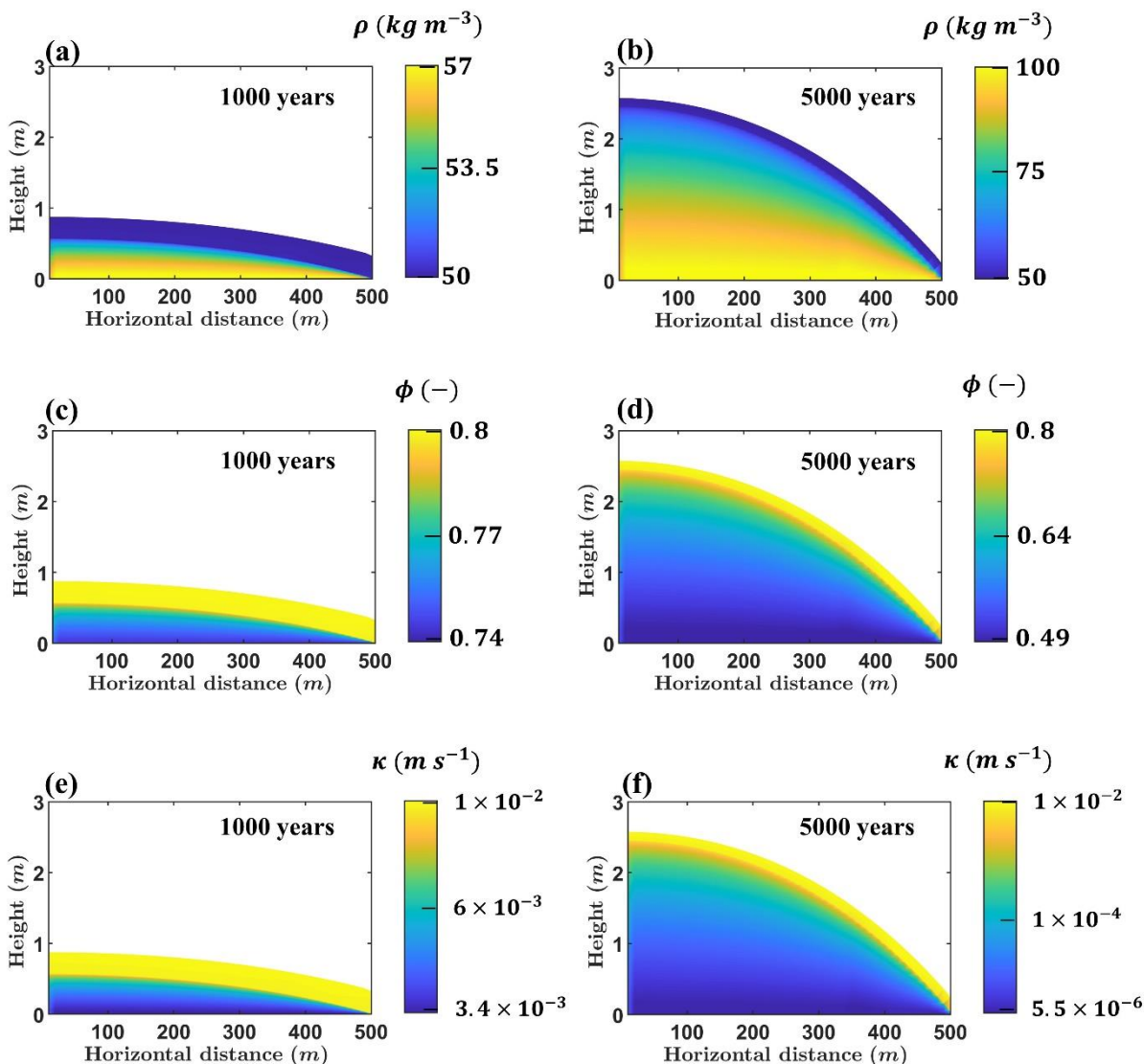
Figure 5: The profiles of (a and b) bulk density, (c and d) active porosity, and (e and f) hydraulic conductivity with spatial variability in the vertical and horizontal directions under constant climate.
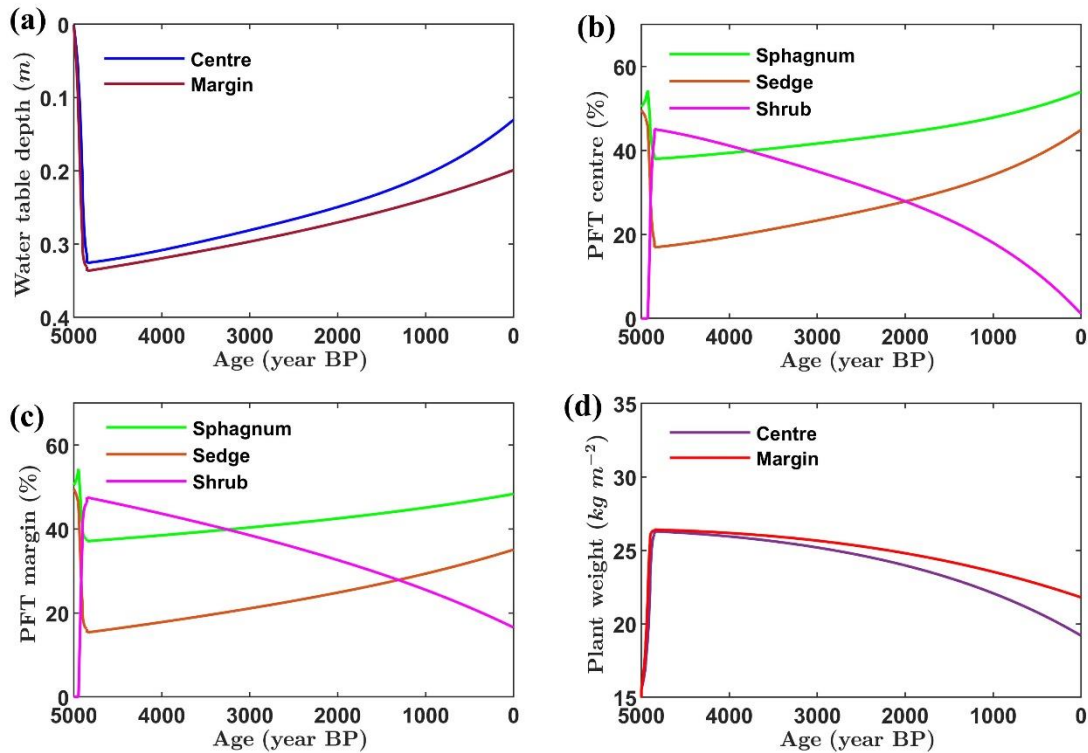
Figure 6: The variations of (a) water table depth, (b) plant functional types (PFT) proportion at the centre, (c) PFT proportion at the margin, and (d) plant weight over 5000 years under constant climate. The centre is defined at the central vertical axis, while the margin is located at a horizontal distance of 500 m from the centre.

Over 5000 years of development, water table depth decreases, resulting in the wetter condition of the peatland (Fig. 6). The difference in the final simulation year between the water table depth at the centre (0.13 m) and at the margin (0.20 m), which is separated by a horizontal distance of 500 m, leads to the variation in vegetation composition and plant weight. The proportion of shrub is lower at the centre compared to the margin, with the value of about 1% and 17%, respectively. In contrast, the sedge and *Sphagnum* proportions reduce from around 45% and 54% at the centre to 35% and 48% at the margin, respectively. The variations in the vegetation composition affect the distribution of plant weight, with the centre (19 kg m^{-2}) providing a lower value of loading than the margin (22 kg m^{-2}).
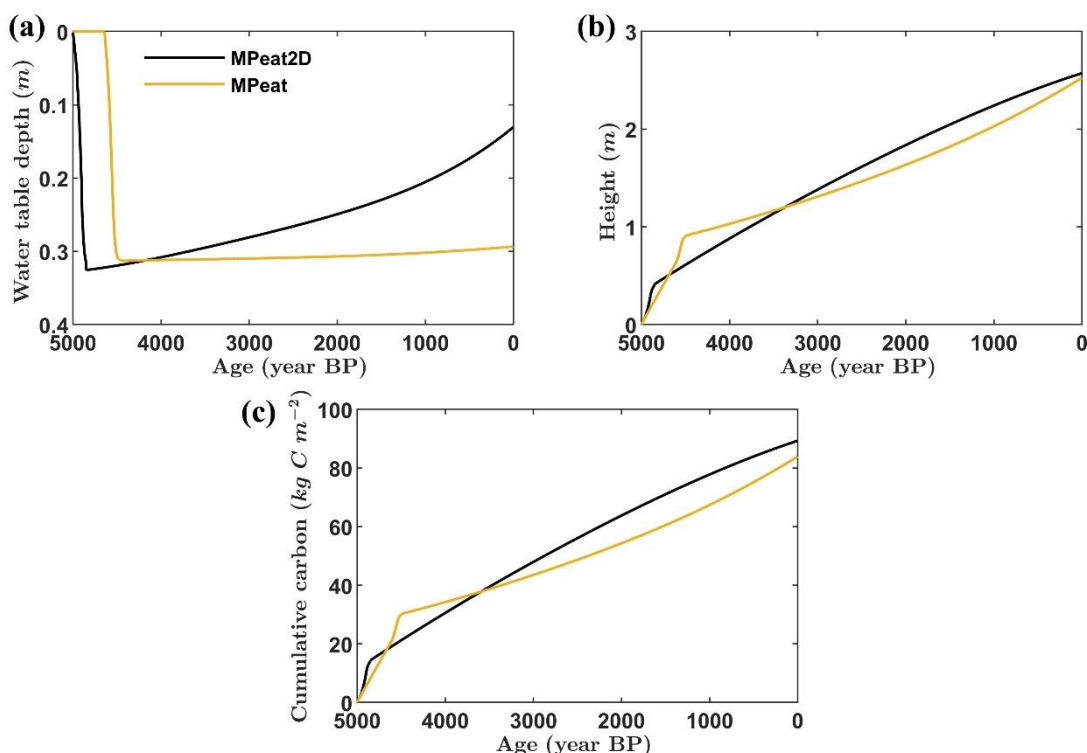
Figure 7: The comparison between MPeat2D and MPeat at the centre for (a) water table depth, (b) peatland height, and (c) cumulative carbon over 5000 years under constant climate.

The comparison between MPeat2D and MPeat is conducted based on the simulation at the centre of the peatland. Under

335   constant climate, the emergence of the unsaturated zone, represented by the non-zero values of water table depth, is faster in the MPeat2D than in the MPeat, with a difference of about 360 years (Fig. 7a). Moreover, the water table depth obtained from MPeat2D (0.13 m) is lower than MPeat (0.3 m) in the final simulation year. Although MPeat2D and MPeat estimate similar peatland height with values of about 2.57 m and 2.52 m (Fig. 7b), respectively, the cumulative carbon obtained from MPeat2D (89 kg C m^{-2}) is higher compared to the MPeat (84 kg C m^{-2}) over 5000 years (Fig. 7c).

340   **4.2 Second group: Non-constant climate**

Under a non-constant climate, the profiles of peat physical properties are similar to those in the constant climate case. The value of bulk density increases while active porosity and hydraulic conductivity decrease from the centre toward the margin (Fig. 8). The main difference is that the range values of bulk density (50 – 104 kg m^3), active porosity (0.47 – 0.8), and hydraulic conductivity (3.7 × 10^{-6} – 1 × 10^{-2} m s^{-1}) are higher in the second group after 5000 years. This condition

345   indicates a more significant effect of mechanical deformation on the peat pore space due to the changing climate.
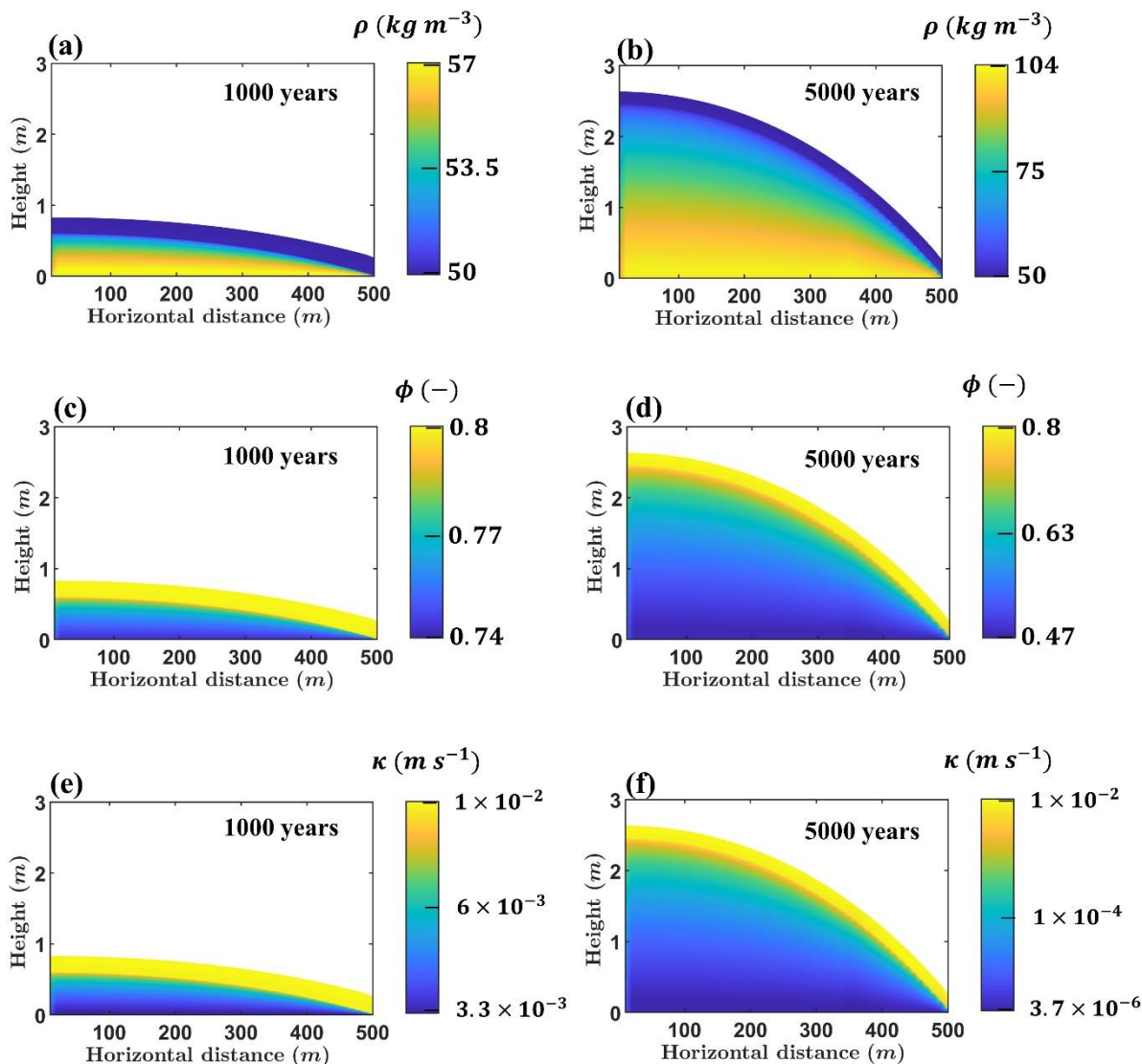
Figure 8: The profiles of (a and b) bulk density, (c and d) active porosity, and (e and f) hydraulic conductivity with spatial variability in the vertical and horizontal directions under non-constant climate.

After the unsaturated zone is developed, around 150 years since peatland initiation, water table depth experiences
350 fluctuations and exhibits lateral variability. The margin, which is located at a horizontal distance of 500 m from the centre, experiences drier conditions indicated by a higher water table depth compared to the centre (Fig. 9). Furthermore, the spatial variability of water table depth results in lateral changes in PFT proportions and plant weight. For example, around 1250 years BP, the water table depth is about 0.07 m at the centre, while at the margin, the water table is located about 0.22 m below the surface. Consequently, the shrub proportion increases from 0% at the centre to 21% at the margin, while
355 sedge and *Sphagnum* decrease from 48% and 52% to 32% and 47% from the centre to the margin, respectively. This

condition produces a spatial variation in plant weight between the centre and the margin with values of about 17 kg m^2 and 22 kg m^2.
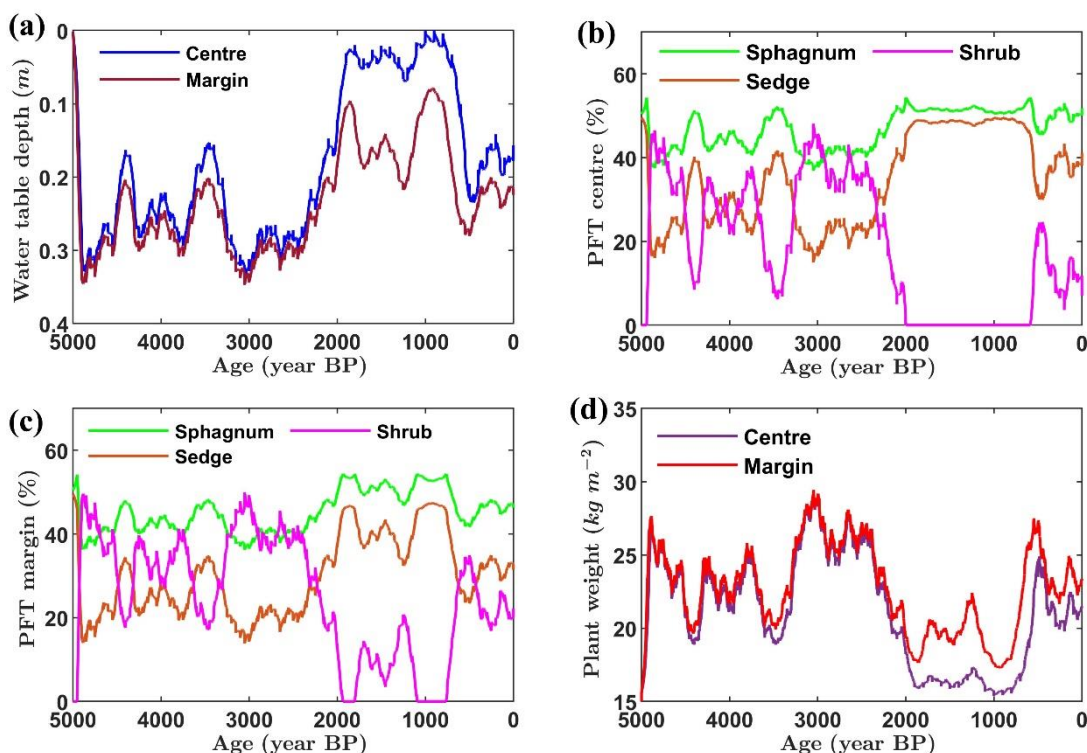
Figure 9: The variations of (a) water table depth, (b) plant functional types (PFT) proportion at the centre, (c) PFT proportion at the margin, and (d) plant weight over 5000 years under non-constant climate. The centre is defined at the central vertical axis, while the margin is located at a horizontal distance of 500 m from the centre.

The comparisons between MPeat2D and MPeat for water table depth, peatland height, and cumulative carbon at the centre area under non-constant climate are shown in Fig. 10. The appearance of the unsaturated zone is around 400 years earlier in the MPeat2D than MPeat based on the non-zero values of the water table depth since peatland initiation. After the unsaturated zone is developed in both models, MPeat2D predicts a lower water table depth compared to the MPeat with the range value of $0 - 0.34$ m and $0.16 - 0.36$ m, respectively. Peatland height and cumulative carbon obtained from MPeat2D around 2.61 m and 92 kg C m^{-2} are more significant than the MPeat estimated values of about 2.39 m and 76 kg C m^{-2}, after 5000 years.
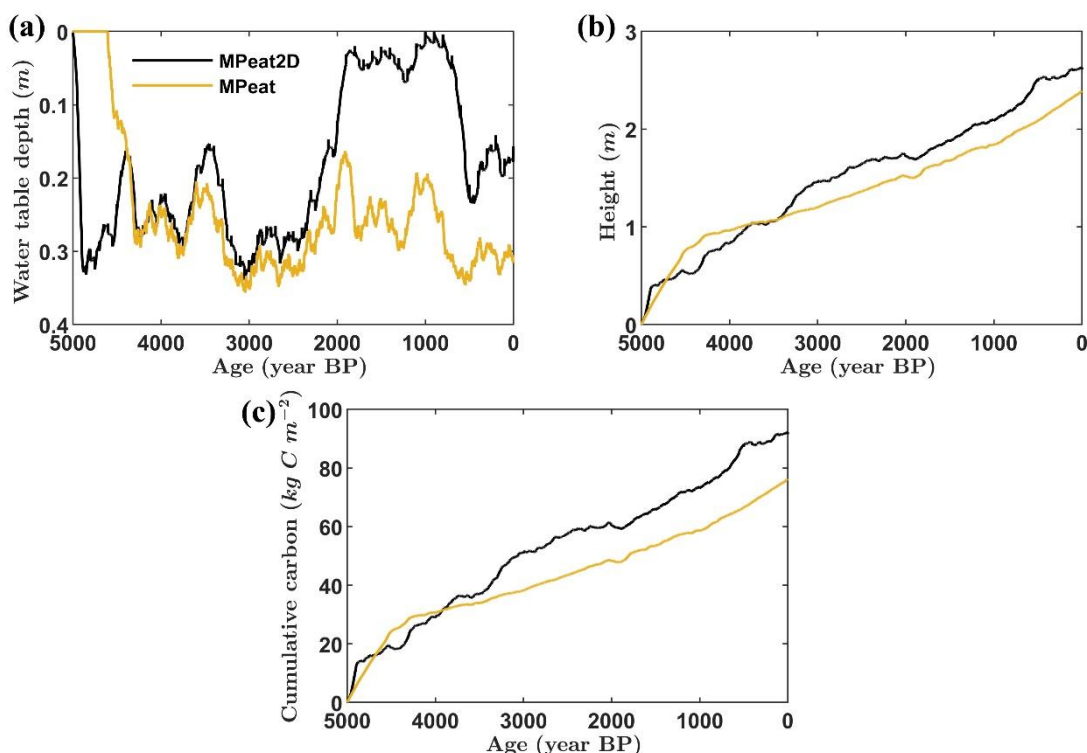
Figure 10: The comparison between MPeat2D and MPeat at the centre for (a) water table depth, (b) peatland height, and (c) cumulative carbon over 5000 years under a non-constant climate.

5 Discussion

The most important result from MPeat2D is the ability to model the influence of spatial variability on long-term peatland behaviour. The addition of the second dimension provides significant impacts on the analysis of peat physical properties because it allows the bulk density, active porosity, and hydraulic conductivity to change in the horizontal and vertical directions. We found that the bulk density increases systematically from the centre to the margin, while the active porosity and hydraulic conductivity experience an opposite pattern with decreasing values from the peatland interior to the edges (Figs. 5 and 8). The horizontal variability of the peat physical properties occurs because the peatland experiences different effects of compaction between the margin and the centre. The steeper hydraulic gradient at the margin promotes water release and reduces the position of the water table (Figs. 6a and 9a) (Reeve et al., 2006; Lewis et al., 2012; Kværner and Snilsberg, 2011; Regan et al., 2019), which results in higher loading from plant weight (Figs. 6d and 9d) and effective stress. In contrast, peatland topography at the centre is mainly flat, leading to the shallow water table position that limits the deformation of the peat pore space.

At smaller scales of a few meters, another possible factor affecting the horizontal variance of peat physical properties is the peatland microform. The measurement from Whittington and Price (2006) indicated that bulk density and hydraulic

conductivity differ substantially in the lateral direction over distances of a few metres between hummocks, lawns, and hollows. Moreover, Baird et al. (2016) showed that the difference in the hydraulic conductivity between contiguous microforms could vary by more than an order of magnitude. The variation in the water table position and plant functional types in the peatland microform (Eppinga et al., 2008; Malhotra et al., 2016; Moore et al., 2019), which significantly affect

390   the loading, effective stress, and compaction on the peat pore space, might become a reasonable explanation for this behaviour. However, Baird et al. (2016) found that the change in hydraulic conductivity is less evident at a deeper location between adjacent hummocks and hollows, which suggests that the lateral variability of hydraulic conductivity at the small scale between the microhabitat types beyond the uppermost peat is equivocal.

The changes of peat physical properties in the vertical direction, from the top surface to the bottom layer, obtained from

395   MPeat2D show an increasing value of bulk density and a decreasing value of active porosity and hydraulic conductivity (Clymo, 1984; Hoag and Price, 1995; Hoag and Price, 1997; Quinton et al., 2008; Quinton et al., 2000; Fraser et al., 2001; Clymo, 2004). The rapid changes occur at the transition between the unsaturated and saturated zones, indicating significant compaction due to the substantial increase of effective stress (Mahdiyasa et al., 2023; Mahdiyasa et al., 2022). The fluctuations of peat physical properties become gradual in the saturated zone because pore water pressure reduces the

400   effective stress and limits the deformation of the peat solid skeleton. Price (2003) found the decreasing value of effective stress below the water table that leads to smaller changes in peat volume, which supports our simulation results.

The inclusion of spatial heterogeneity provides crucial feedback on peat thickness and carbon stock, as shown by the comparison between MPeat2D and MPeat (Figs. 7 and 10). MPeat2D simulates spatial variations in the peat physical properties and produces a non-uniform hydraulic gradient, including a lower hydraulic conductivity at the margin and nearly

405   flat topography at the centre, which supports the water accumulation. In contrast, as a 1D model, MPeat assumes constant peat physical properties in the lateral direction and a uniform hydraulic gradient, resulting in the omission of peatland processes that affect the water balance. Consequently, MPeat2D simulates a shallower water table position than MPeat, leading to the shorter residence time of organic matter in the unsaturated zone and providing positive feedback on the peat and carbon accumulation (Evans et al., 2021; Huang et al., 2021; Ma et al., 2022). The differences between MPeat2D and

410   MPeat are more pronounced under a non-constant climate (Fig. 10), indicating the potential importance of spatial variability to understand the influence of climate change on the peatland carbon balance and resilience.

Our simulation results are in agreement with Lapen et al. (2005), who found that lateral variations of hydraulic conductivity encourage water accumulation and produce a more significant peat thickness. However, Lapen et al. (2005) finding is constructed based on the sensitivity analysis of the groundwater flow model at steady-state conditions, which omits the

415   complex feedback from the peatland. Conversely, MPeat2D provides a comprehensive approach incorporating mechanical, ecological, and hydrological feedback to highlight the influence of spatial variations of physical properties and water table position on the peat and carbon accumulation during development process.

5.1 Comparison with field measurements

We compare the simulation results from MPeat2D under a non-constant climate that provides a more realistic condition with
420   field observation for peat physical properties, peat thickness, and carbon accumulation. The comparison of peat physical
properties is conducted in the horizontal and vertical directions due to the spatial heterogeneity of bulk density, active
porosity, and hydraulic conductivity. In the horizontal direction, we use the data from Lewis et al. (2012), who measured the
lateral variabilities of hydraulic conductivity and bulk density at a depth of 30 to 40 cm from a blanket peatland in Ireland as
a comparison. Lewis et al. (2012) found that the average values of hydraulic conductivity at the margin and the centre are
425   around 10^{-6} and 10^{-4} m s^{-1}, respectively. After 5000 years of development, MPeat2D produces hydraulic conductivity
(Fig. 8f) with a similar value at the margin (6.4×10^{-6} m s^{-1}) but higher at the centre (1.3×10^{-3} m s^{-1}) compared to the
Lewis et al. (2012) observations. Moreover, the bulk density values obtained from Lewis et al. (2012) are around 55 and
110 kg m^{-3}, while our simulation (Fig. 8b) provides values of about 59 and 101 kg m^{-3} at the centre and margin,
respectively. In the vertical direction, the changes in bulk density simulated from MPeat2D (Fig. 8b) are in the range of
430   50 – 104 kg m^3, consistent with the reported measurements of bulk density about $30 - 120$ kg m^3 (Lunt et al., 2019; Loisel
et al., 2014; Clymo, 1984). Furthermore, the simulation results of active porosity (Fig. 8d) and hydraulic conductivity (Fig.
8f) fluctuate between $0.47 - 0.8$ and $3.7 \times 10^{-6} - 1 \times 10^{-2}$ m s^{-1}, which are in accord with the field observations of
active porosity and hydraulic conductivity about $0.1 - 0.8$ and $7 \times 10^{-9} - 1.6 \times 10^{-2}$ m s^{-1}, respectively (Quinton et al.,
2008; Quinton et al., 2000; Clymo, 2004; Fraser et al., 2001; Hoag and Price, 1997; Hoag and Price, 1995). Therefore, in
435   general, MPeat2D can model the spatial variability of peat physical properties in the horizontal and vertical directions with
reasonable outputs. The discrepancies between simulation results and the field measurement mainly related to the site
specific characteristics, including peat stiffness, PFT composition, and substrate topography that result in the variations of
compaction effect (Mahdiyasa et al., 2023; Mahdiyasa et al., 2022; Whittington et al., 2007; Malmer et al., 1994).

The peat thickness and carbon accumulation rate obtained from MPeat2D appear to be realistic. MPeat2D produces an
440   average growth rate of about 0.52 mm yr^{-1}, which leads to a height of 2.61 m after 5000 years (Fig. 10b). Charman (2002)
found that the average growth rates of the blanket and raised peatland are about 0.65 and 1 mm yr^{-1}, respectively, based on
the relation between peatland carbon accumulation and age-depth curves. Aaby and Tauber (1975) analysed the correlation
between the rate of peat accumulation and the degree of humification that produced the growth rate of raised peatland in the
range of $0.16 - 0.80$ mm yr^{-1} with an average value of 0.44 mm yr^{-1}. Aaby and Tauber (1975) suggested that the
445   relationship between the degree of humification and the growth rate is affected significantly by mechanical compaction. A
more decomposed peat experiences a higher compaction effect due to the reduction in Young's modulus and strength
(Mahdiyasa et al., 2023; Mahdiyasa et al., 2022), which results in a lower peat thickness. Furthermore, the average value of
the net rate of carbon accumulation obtained from MPeat2D is about 0.0183 kg C m^{-2} yr^{-1} (Fig. 10c), which is in
agreement with the reported measurements of northern peatlands during the Holocene with an average value around
450   0.0186 kg C m^{-2} yr^{-1} (Yu et al., 2010; Yu et al., 2009).
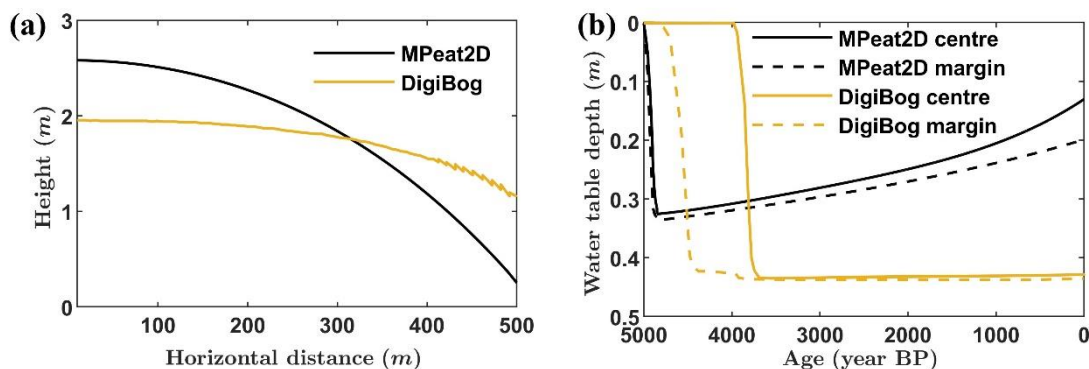
Figure 11: The comparison between MPeat2D and DigiBog Bog 2 (Morris et al., 2012) for (a) peatland shape and (b) water table depth over 5000 years. Both models assume that the peatland develops above the flat and impermeable substrate with constant climate.

455 **5.2 Comparison with the other two-dimensional peatland development model**

We emphasise the critical function of mechanical-ecohydrological feedback to simulate peatland development in 2D by comparing MPeat2D with the other ecohydrological model DigiBog (Baird et al., 2012; Morris et al., 2012). Using the same assumption of the flat and impermeable substrate with constant climate, both models produce dome shapes of the peatland over 5000 years (Fig. 11a). However, the inclusion of mechanical-ecohydrological feedback on MPeat2D provides a

460 plausible profile of bulk density (Fig. 5b) and active porosity (Fig. 5d) that are assumed to be a constant by DigiBog. The changes in peat physical properties and the discrepancy in the hydraulic gradient obtained from MPeat2D lead to the spatial variation of water table depth, which is in line with the field observations (Reeve et al., 2006; Lewis et al., 2012; Kværner and Snilsberg, 2011; Regan et al., 2019). Furthermore, the water table depth decreases as the peatland develops in the MPeat2D, resulting in wetter conditions of the peatland due to a more significant effect of compaction that supports the

465 water accumulation (Fig. 11b). Contrastingly, DigiBog produces a relatively uniform hydraulic gradient, leading to the constant water table depth between the centre and the margin during the simulation period. This condition limits the capabilities of DigiBog to analyse the lateral variation in peat production, decomposition, and PFT proportion because these peatland characteristics depend on the water table depth (Clymo, 1984; Belyea and Clymo, 2001; Moore et al., 2002; Kokkonen et al., 2019; Laine et al., 2021).

470 The inclusion of mechanical-ecohydrological feedback also produces a more plausible shape of the peatland in 2D. Although MPeat2D suffers from the appearance of a cliff at the margin as DigiBog (Fig. 11a), the influence of mechanical compaction on the MPeat2D results in a lower cliff height than DigiBog, with values of about 0.27 m compared to 1.15 m, respectively. The peat cliff at the margin does not appear in the natural condition except due to extraction or erosion (Tuukkanen et al., 2017; Tarvainen et al., 2022). Furthermore, the continuum concept (Irgens, 2008; Jog, 2015) employed by MPeat2D

475 produces continuous deformation of peat pore space, resulting in the smoother profile of peatland shape, especially near the margin, compared to DigiBog that uses linked vertical column (Fig. 11a). However, MPeat2D assumes a uniform

distribution of peat throughout the fixed horizontal domain in the initial stages of development, which prevents MPeat2D from modelling the lateral expansion. In contrast, DigiBog can capture the lateral growth of the peatland from the margin toward the centre (Morris et al., 2012).

5.3 Limitations and future development

480

Lateral expansion is crucial to model the paludification process that influences peatland behaviour because the transition process from forest to peatland involves changes in vegetation, nutrient availability, and peat physical properties (Charman, 2002; Anderson et al., 2003; Rydin and Jeglum, 2006). Peatland lateral expansion requires an evolving domain that results in moving boundary problems (Tezduyar, 2001; Gawlik and Lew, 2015). Simplifying assumptions may be necessary to involve

485 the moving boundary conditions into MPeat2D, including providing the rate of lateral expansion that determines the boundary motion and the changing domain. Moreover, to improve the numerical stability of the model, a smaller grid size might be required, particularly around the boundaries, due to significant differences in the internal stresses.

The assumption of a flat substrate employed by MPeat2D could be improved by introducing a more general landscape condition consisting of upland, sloping area, and lowland based on the theoretical landscape model proposed by Winter

490 (2001). The landscape variations, together with the feedback from mechanical, ecological, and hydrological processes, affect the stresses on the peat body that control the occurrence of failure conditions on the peatland. The peatland failure involving mass movement (Dykes and Selkirk-Bell, 2010; Dykes, 2022; Dykes, 2008) influences the estimation of carbon accumulation on the peatland because it might result in the formation of water channels that facilitate the drainage and oxidation processes (Warburton et al., 2003; Evans and Warburton, 2007). Potentially, this phenomenon could determine the

495 maximum limit to peatland carbon accumulation in a landscape (Large et al., 2021).

The current version of MPeat2D is focused on modelling raised ombrotrophic peatland, which grows in temperate climates. However, it should be possible to develop MPeat2D to model the other peatland types, for example, the tropical peatland. Modifications of some processes are required before applying MPeat2D to analyse the peatland in tropical areas, including the variation in the rate of peat production, peat physical properties characteristics, and loading behaviour. MPeat2D uses the

500 empirical relationship between peat production and water table depth, which is formulated based on the data from Ellergower Moss, Scotland (Belyea and Clymo, 2001). The rate of peat production in the tropical peatland should be different from the northern temperate peatland due to the variations in the vegetation composition. The hydraulic conductivity of tropical peatlands is relatively high compared to the northern temperate peatland, which affects the water table position (Baird et al., 2017). Moreover, the loading from trees and the influence of roots for maintaining mechanical

505 stability are significant processes in tropical peatlands, which requires an additional formulation in the MPeat2D mechanical submodel.

Finally, the development of MPeat2D into a three-dimensional (3D) model provides a more comprehensive analysis of the peatland carbon accumulation process and phenomena that require explicit spatial interactions in 3D. The comparison between MPeat2D and MPeat indicates the crucial function of adding a second dimension to estimate peatland carbon

510 accumulation. MPeat2D produces greater cumulative carbon, particularly under non-constant climate, due to the lateral variability of water table depth and peat physical properties incorporated by the 2D model. Based on this preliminary result, it might be possible that a 3D model of peatland development might result in a more significant carbon accumulation than the 1D or 2D models because of the more complex feedback mechanisms involved by a higher dimensional model. The 3D model is also required to understand the patterning phenomena on the peatland surface, which is highly directional and

515 affected by spatial characteristics. The analysis of surface patterning is typically developed based on ecohydrological feedback, which encompasses the interactions between water table position, vegetation communities, nutrient availability, and peat hydraulic properties (Eppinga et al., 2009; Eppinga et al., 2008; Morris et al., 2013; Béguin et al., 2019). However, as a porous medium with relatively low shear and tensile strength (Long, 2005; Boylan et al., 2008; O'kelly, 2017; Dykes, 2008), mechanical instability also determines the process of surface patterning on the peatland. The simulation from Briggs

520 et al. (2007) indicates that the peatland surface might experience wrinkles due to the changing pattern between tensile and compressive stresses. Therefore, a fully coupled mechanical, ecological, and hydrological model of peatland growth in three dimensions might be suitable for analysing the appearance and impact of surface patterning on the peatland water flow and carbon balance.

6 Conclusion

525 MPeat2D is a two-dimensional peatland growth model that incorporates mechanical-ecohydrological feedback and the influence of spatial variability on peatland behaviour. This model is developed based on the poroelasticity and continuum concept, resulting in the plausible outputs of peat physical properties, water table position, and vegetation composition. MPeat2D produces a higher bulk density and lower active porosity and hydraulic conductivity at the margin compared to the centre due to the different effects of compaction, which are in accord with field observations. Furthermore, lateral variability

530 of water table depth because of the changes in the hydraulic gradient leads to different vegetation compositions between the margin and the centre. The comparison between MPeat2D and the other peatland growth models, MPeat and DigiBog, indicates the critical function of mechanical, ecological, and hydrological processes together with the feedback from spatial heterogeneity on the peatland shape, carbon stock and resilience.

Code availability

535 The codes that support the findings of this study are openly available in zenodo at https://doi.org/10.5281/zenodo.10050891 (Mahdiyasa, 2023)

Author contribution

AWM and DJL conceptualised and designed the research. AWM developed the model, performed the simulations, and prepared the initial manuscript. DJL, MI, and BPM provided advice on the model interpretation and contributed to the
540   editing and reviewing of the manuscript. BPM provided financial support and computing resources for the simulations.

Competing interests

The authors declare that they have no conflict of interest.

Acknowledgements

This work was funded by LPDP RISPRO-UKICIS (United Kingdom-Indonesia Consortium for Interdisciplinary Sciences)
545   green economy with grant number 4345/E4/AL.04.

References

Aaby, B. and Tauber, H.: Rates of peat formation in relation to degree of humification and local environment, as shown by studies of a raised bog in Deninark, Boreas, 4, 1-17, https://doi.org/10.1111/j.1502-3885.1975.tb00675.x, 1975.

Abousleiman, Y., Cheng, A. H.-D., Cui, L., Detournay, E., and Roegiers, J.-C.: Mandel's problem revisited, Géotechnique, 46, 187-195, https://doi.org/10.1680/geot.1996.46.2.187, 1996.

Anderson, R. L., Foster, D. R., and Motzkin, G.: Integrating lateral expansion into models of peatland development in temperate New England, Journal of Ecology, 91, 68-76, https://doi.org/10.1046/j.1365-2745.2003.00740.x, 2003.

Armstrong, A. C.: Hydrological model of peat-mound form with vertically varying hydraulic conductivity, Earth Surface Processes and Landforms, 20, 473-477, https://doi.org/10.1002/esp.3290200508, 1995.

Baird, A. J., Eades, P. A., and Surridge, B. W. J.: The hydraulic structure of a raised bog and its implications for ecohydrological modelling of bog development, Ecohydrology, 1, 289-298, https://doi.org/10.1002/eco.33, 2008.

Baird, A. J., Morris, P. J., and Belyea, L. R.: The DigiBog peatland development model 1: rationale, conceptual model, and hydrological basis, Ecohydrology, 5, 242-255, https://doi.org/10.1002/eco.230, 2012.

Baird, A. J., Milner, A. M., Blundell, A., Swindles, G. T., and Morris, P. J.: Microform-scale variations in peatland permeability and their ecohydrological implications, Journal of Ecology, 104, 531-544, https://doi.org/10.1111/1365-2745.12530, 2016.

Baird, A. J., Low, R., Young, D., Swindles, G. T., Lopez, O. R., and Page, S.: High permeability explains the vulnerability of the carbon store in drained tropical peatlands, Geophysical Research Letters, 44, 1333-1339, https://doi.org/10.1002/2016GL072245, 2017.

Ballard, C. E., McIntyre, N., Wheater, H. S., Holden, J., and Wallage, Z. E.: Hydrological modelling of drained blanket peatland, Journal of Hydrology, 407, 81-93, https://doi.org/10.1016/j.jhydrol.2011.07.005, 2011.

Béguin, C., Brunetti, M., and Kasparian, J.: Quantitative analysis of self-organized patterns in ombrotrophic peatlands, Scientific Reports, 9, 1499, https://doi.org/10.1038/s41598-018-37736-8, 2019.

Belyea, L. R. and Clymo, R. S.: Feedback control of the rate of peat formation, Proceedings of the Royal Society of London. Series B: Biological Sciences, 268, 1315-1321, https://doi.org/10.1098/rspb.2001.1665, 2001.

Biot, M. A.: General theory of three-dimensional consolidation, Journal of Applied Physics, 12, 155-164, https://doi.org/10.1063/1.1712886, 1941.

Borren, W. and Bleuten, W.: Simulating Holocene carbon accumulation in a western Siberian watershed mire using a three-dimensional dynamic modeling approach, Water Resources Research, 42, https://doi.org/10.1029/2006WR004885, 2006.

Boussinesq, J.: Théorie de l'intumescence liquide, applelée onde solitaire ou de translation, se propageant dans un canal rectangulaire, Comptes Rendus de l'Académie des Sciences., 72, 1871.

Boylan, N., Jennings, P., and Long, M.: Peat slope failure in Ireland, Quarterly Journal of Engineering Geology and Hydrogeology, 41, 93-108, https://doi.org/10.1144/1470-9236/06-028, 2008.

Briggs, J., Large, D. J., Snape, C., Drage, T., Whittles, D., Cooper, M., Macquaker, J. H. S., and Spiro, B. F.: Influence of climate and hydrology on carbon in an early Miocene peatland, Earth and Planetary Science Letters, 253, 445-454, https://doi.org/10.1016/j.epsl.2006.11.010, 2007.

Charman, D.: Peatlands and Environmental Change, John Wiley and Sons Ltd., Chichester, 2002.

Cheng, A. H. D.: A linear constitutive model for unsaturated poroelasticity by micromechanical analysis, International Journal for Numerical and Analytical Methods in Geomechanics, 44, 455-483, https://doi.org/10.1002/nag.3033, 2020.

Cheng, A. H. D. and Detournay, E.: A direct boundary element method for plane strain poroelasticity, International Journal for Numerical and Analytical Methods in Geomechanics, 12, 551-572, https://doi.org/10.1002/nag.1610120508, 1988.

Clymo, R. S.: The limits to peat bog growth, Philosophical Transactions of the Royal Society of London. B, Biological Sciences, 303, 605-654, https://doi.org/10.1098/rstb.1984.0002, 1984.

Clymo, R. S.: Hydraulic conductivity of peat at Ellergower Moss, Scotland, Hydrological Processes, 18, 261-274, https://doi.org/10.1002/hyp.1374, 2004.

Cobb, A. R., Hoyt, A. M., Gandois, L., Eri, J., Dommain, R., Abu Salim, K., Kai, F. M., Haji Su'ut, N. S., and Harvey, C. F.: How temporal patterns in rainfall determine the geomorphology and carbon fluxes of tropical peatlands, Proceedings of the National Academy of Sciences, 114, E5187-E5196, https://doi.org/10.1073/pnas.1701090114, 2017.

Coussy, O.: Poromechanics, John Wiley & Sons Ltd, Chichester, United Kingdom, 2004.

de Boer, R.: Theory of Porous Media, Springer, Berlin, Heidelberg, Germany, https://doi.org/10.1007/978-3-642-59637-7, 2000.

Detournay, E. and Cheng, A. H. D.: Fundamentals of Poroelasticity, in: Analysis and Design Methods, edited by: Fairhurst, C., Pergamon, Oxford, 113-171, 10.1016/B978-0-08-040615-2.50011-3, 1993.

Duijn, C. J. v. and Mikelic, A.: Mathematical Proof of the Mandel--Cryer Effect in Poroelasticity, Multiscale Modeling & Simulation, 19, 550-567, https://doi.org/10.1137/20m1346043, 2021.

Dupuit, J.: Etudes theoriques et pratiques sur le mouvement des eaux dans les canaux decouverts et a travers les terrains permeabls: avec des considerations relatives au regime des grandes eaux, au debouche a leur donner, et a la marche des alluvions dans les rivie`res a fond mobile., Dunod, Paris, France, 1863.

Dykes, A. P.: Tensile strength of peat: laboratory measurement and role in Irish blanket bog failures, Landslides, 5, 417-429, https://doi.org/10.1007/s10346-008-0136-1, 2008.

Dykes, A. P.: Recent peat slide in Co. Antrim extends the known range of weak basal peat across Ireland, Environmental Geotechnics, 9, 22-35, https://doi.org/10.1680/jenge.17.00088, 2022.

Dykes, A. P. and Selkirk-Bell, J. M.: Landslides in blanket peat on subantarctic islands: causes, characteristics and global significance, Geomorphology, 124, 215-228, https://doi.org/10.1016/j.geomorph.2010.09.002, 2010.

Dykes, A. P. and Warburton, J.: Failure of peat-covered hillslopes at Dooncarton Mountain, Co. Mayo, Ireland: analysis of topographic and geotechnical factors, CATENA, 72, 129-145, https://doi.org/10.1016/j.catena.2007.04.008, 2008.

Edelsbrunner, H.: Geometry and Topology for Mesh Generation, Cambridge University Press,, Cambridge, United Kingdom, 2001.

Eppinga, M. B., Rietkerk, M., Wassen, M. J., and De Ruiter, P. C.: Linking Habitat Modification to Catastrophic Shifts and Vegetation Patterns in Bogs, Plant Ecology, 200, 53-68, https://doi.org/10.1007/s11258-007-9309-6, 2009.

Eppinga, M. B., Rietkerk, M., Borren, W., Lapshina, E. D., Bleuten, W., and Wassen, M. J.: Regular Surface Patterning of Peatlands: Confronting Theory with Field Data, Ecosystems, 11, 520-536, https://doi.org/10.1007/s10021-008-9138-z, 2008.

Evans, C. D., Peacock, M., Baird, A. J., Artz, R. R. E., Burden, A., Callaghan, N., Chapman, P. J., Cooper, H. M., Coyle, M., Craig, E., Cumming, A., Dixon, S., Gauci, V., Grayson, R. P., Helfter, C., Heppell, C. M., Holden, J., Jones, D. L., Kaduk, J., Levy, P., Matthews, R., McNamara, N. P., Misselbrook, T., Oakley, S., Page, S. E., Rayment, M., Ridley, L. M., Stanley, K. M., Williamson, J. L., Worrall, F., and Morrison, R.: Overriding water table control on managed peatland greenhouse gas emissions, Nature, 593, 548-552, https://doi.org/10.1038/s41586-021-03523-1, 2021.

Evans, M. and Warburton, J.: Geomorphology of Upland Peat: Erosion, Form and Landscape Change, John Wiley & Sons Ltd, 2007.

Forchheimer, P.: Hydraulik (3 auflage), B. G. Teubner, Berlin, 1930.

Fraser, C. J. D., Roulet, N. T., and Moore, T. R.: Hydrology and dissolved organic carbon biogeochemistry in an ombrotrophic bog, Hydrological Processes, 15, 3151-3166, https://doi.org/10.1002/hyp.322, 2001.

Gawlik, E. S. and Lew, A. J.: Unified Analysis of Finite Element Methods for Problems with Moving Boundaries, SIAM Journal on Numerical Analysis, 53, 2822-2846, https://doi.org/10.1137/140990437, 2015.

George, P.-L.: Mesh Generation – Application to Finite Elements, Hermes Science Publishing, Paris, 2000.

Glaser, P. H., Hansen, B. C. S., Siegel, D. I., Reeve, A. S., and Morin, P. J.: Rates, pathways and drivers for peatland development in the Hudson Bay Lowlands, northern Ontario, Canada, Journal of Ecology, 92, 1036-1053, https://doi.org/10.1111/j.0022-0477.2004.00931.x, 2004.

Hoag, R. S. and Price, J. S.: A field-scale, natural gradient solute transport experiment in peat at a Newfoundland blanket bog, Journal of Hydrology, 172, 171-184, https://doi.org/10.1016/0022-1694(95)02696-M, 1995.

Hoag, R. S. and Price, J. S.: The effects of matrix diffusion on solute transport and retardation in undisturbed peat in laboratory columns, Journal of Contaminant Hydrology, 28, 193-205, https://doi.org/10.1016/S0169-7722(96)00085-X, 1997.

650 Hogan, J. M., van der Kamp, G., Barbour, S. L., and Schmidt, R.: Field methods for measuring hydraulic properties of peat deposits, Hydrological Processes, 20, 3635-3649, https://doi.org/10.1002/hyp.6379, 2006.

Huang, Y., Ciais, P., Luo, Y., Zhu, D., Wang, Y., Qiu, C., Goll, D. S., Guenet, B., Makowski, D., De Graaf, I., Leifeld, J., Kwon, M. J., Hu, J., and Qu, L.: Tradeoff of CO2 and CH4 emissions from global peatlands under water-table drawdown, Nature Climate Change, 11, 618-622, https://doi.org/10.1038/s41558-021-01059-w, 2021.

Ingram, H. A. P.: Size and shape in raised mire ecosystems: a geophysical model, Nature, 297, 300-303, 655 https://doi.org/10.1038/297300a0, 1982.

Irgens, F.: Continuum Mechanics, Springer-Verlag Berlin, Heidelberg, 661 pp., https://doi.org/10.1007/978-3-540-74298-2, 2008.

Jha, B. and Juanes, R.: Coupled multiphase flow and poromechanics: A computational model of pore pressure effects on fault slip and earthquake triggering, Water Resources Research, 50, 3776-3808, 660 https://doi.org/10.1002/2013WR015175, 2014.

Jog, C. S.: Continuum Mechanics: Volume 1: Foundations and Applications of Mechanics 3rd, Cambridge University Press, Cambridge, 2015.

Kettridge, N., Turetsky, M. R., Sherwood, J. H., Thompson, D. K., Miller, C. A., Benscoter, B. W., Flannigan, M. D., Wotton, B. M., and Waddington, J. M.: Moderate drop in water table increases peatland vulnerability to post-fire 665 regime shift, Scientific Reports, 5, 8063, https://doi.org/10.1038/srep08063, 2015.

Kokkonen, N. A. K., Laine, A. M., Laine, J., Vasander, H., Kurki, K., Gong, J., and Tuittila, E.-S.: Responses of peatland vegetation to 15-year water level drawdown as mediated by fertility level, Journal of Vegetation Science, 30, 1206-1216, https://doi.org/10.1111/jvs.12794, 2019.

Korhola, A., Alm, J., Tolonen, K., Turunen, J., and Jungner, H.: Three-dimensional reconstruction of carbon accumulation 670 and CH4 emission during nine millennia in a raised mire, Journal of Quaternary Science, 11, https://doi.org/10.1002/(SICI)1099-1417(199603/04)11:2<161::AID-JQS248>3.0.CO;2-J, 1996.

Kværner, J. and Snilsberg, P.: Groundwater hydrology of boreal peatlands above a bedrock tunnel – Drainage impacts and surface water groundwater interactions, Journal of Hydrology, 403, 278-291, https://doi.org/10.1016/j.jhydrol.2011.04.006, 2011.

675 Laine, A. M., Korrensalo, A., Kokkonen, N. A. K., and Tuittila, E.-S.: Impact of long-term water level drawdown on functional plant trait composition of northern peatlands, Functional Ecology, 35, 2342-2357, https://doi.org/10.1111/1365-2435.13883, 2021.

Lapen, D. R., Price, J. S., and Gilbert, R.: Modelling two-dimensional steady-state groundwater flow and flow sensitivity to boundary conditions in blanket peat complexes, Hydrological Processes, 19, 371-386, 680 https://doi.org/10.1002/hyp.1507, 2005.

Large, D. J., Marshall, C., Jochmann, M., Jensen, M., Spiro, B. F., and Olaussen, S.: Time, Hydrologic Landscape, and the Long-Term Storage of Peatland Carbon in Sedimentary Basins, Journal of Geophysical Research: Earth Surface, 126, e2020JF005762, https://doi.org/10.1029/2020JF005762, 2021.

Lewis, C., Albertson, J., Xu, X., and Kiely, G.: Spatial variability of hydraulic conductivity and bulk density along a blanket 685 peatland hillslope, Hydrological Processes, 26, 1527-1537, https://doi.org/10.1002/hyp.8252, 2012.

Loisel, J., Yu, Z., Beilman, D. W., Camill, P., Alm, J., Amesbury, M. J., Anderson, D., Andersson, S., Bochicchio, C., Barber, K., Belyea, L. R., Bunbury, J., Chambers, F. M., Charman, D. J., De Vleeschouwer, F., Fiałkiewicz-Kozieł, B., Finkelstein, S. A., Gałka, M., Garneau, M., Hammarlund, D., Hinchcliffe, W., Holmquist, J., Hughes, P., Jones, M. C., Klein, E. S., Kokfelt, U., Korhola, A., Kuhry, P., Lamarre, A., Lamentowicz, M., Large, D., Lavoie, M., 690 MacDonald, G., Magnan, G., Mäkilä, M., Mallon, G., Mathijssen, P., Mauquoy, D., McCarroll, J., Moore, T. R., Nichols, J., O'Reilly, B., Oksanen, P., Packalen, M., Peteet, D., Richard, P. J., Robinson, S., Ronkainen, T., Rundgren, M., Sannel, A. B. K., Tarnocai, C., Thom, T., Tuittila, E.-S., Turetsky, M., Väliranta, M., van der Linden, M., van Geel, B., van Bellen, S., Vitt, D., Zhao, Y., and Zhou, W.: A database and synthesis of northern peatland soil properties and Holocene carbon and nitrogen accumulation, The Holocene, 24, 1028-1042, 695 https://doi.org/10.1177/0959683614538073, 2014.

Long, M.: Review of peat strength, peat characterisation and constitutive modelling of peat with reference to landslides, Studia Geotechnica et Mechanica, 27, 67-90, 2005.

Lunt, P. H., Fyfe, R. M., and Tappin, A. D.: Role of recent climate change on carbon sequestration in peatland systems, Science of The Total Environment, 667, 348-358, https://doi.org/10.1016/j.scitotenv.2019.02.239, 2019.

700 Ma, L., Zhu, G., Chen, B., Zhang, K., Niu, S., Wang, J., Ciais, P., and Zuo, H.: A globally robust relationship between water table decline, subsidence rate, and carbon release from peatlands, Communications Earth & Environment, 3, 254, https://doi.org/10.1038/s43247-022-00590-8, 2022.

Mahdiyasa, A. W.: MPeat2D (1.0), Zenodo [code], https://doi.org/10.5281/zenodo.10050891, 2023.

Mahdiyasa, A. W., Large, D. J., Muljadi, B. P., and Icardi, M.: Modelling the influence of mechanical-ecohydrological
705 feedback on the nonlinear dynamics of peatlands, Ecological Modelling, 478, 110299, https://doi.org/10.1016/j.ecolmodel.2023.110299, 2023.

Mahdiyasa, A. W., Large, D. J., Muljadi, B. P., Icardi, M., and Triantafyllou, S.: MPeat—A fully coupled mechanical-ecohydrological model of peatland development, Ecohydrology, 15, e2361, https://doi.org/10.1002/eco.2361, 2022.

Malhotra, A., Roulet, N. T., Wilson, P., Giroux-Bougard, X., and Harris, L. I.: Ecohydrological feedbacks in peatlands: an
710 empirical test of the relationship among vegetation, microtopography and water table, Ecohydrology, 9, 1346-1357, https://doi.org/10.1002/eco.1731, 2016.

Malmer, N., Svensson, B. M., and Wallén, B.: Interactions between Sphagnum mosses and field layer vascular plants in the development of peat-forming systems, Folia Geobotanica & Phytotaxonomica, 29, 483-496, https://doi.org/10.1007/BF02883146, 1994.

715 Mandel, J.: Consolidation Des Sols (Étude Mathématique), Géotechnique, 3, 287-299, https://doi.org/10.1680/geot.1953.3.7.287, 1953.

McNeil, P. and Waddington, J. M.: Moisture controls on Sphagnum growth and CO2 exchange on a cutover bog, Journal of Applied Ecology, 40, 354-367, https://doi.org/10.1046/j.1365-2664.2003.00790.x, 2003.

Mesri, G. and Ajlouni, M.: Engineering properties of fibrous peats, Journal of Geotechnical and Geoenvironmental
720 Engineering, 133, 850-866, https://doi.org/10.1061/(ASCE)1090-0241(2007)133:7(850), 2007.

Moore, P. A., Lukenbach, M. C., Thompson, D. K., Kettridge, N., Granath, G., and Waddington, J. M.: Assessing the peatland hummock–hollow classification framework using high-resolution elevation models: implications for appropriate complexity ecosystem modeling, Biogeosciences, 16, 3491-3506, https://doi.org/10.5194/bg-16-3491-2019, 2019.

725 Moore, T. R., Bubier, J. L., Frolking, S. E., Lafleur, P. M., and Roulet, N. T.: Plant biomass and production and CO2 exchange in an ombrotrophic bog, Journal of Ecology, 90, 25-36, https://doi.org/10.1046/j.0022-0477.2001.00633.x, 2002.

Moore, T. R., Trofymow, J. A., Siltanen, M., Prescott, C., and Group, C. W.: Patterns of decomposition and carbon, nitrogen, and phosphorus dynamics of litter in upland forest and peatland sites in central Canada, Canadian Journal
730 of Forest Research, 35, 133-142, https://doi.org/10.1139/x04-149, 2005.

Morris, P. J., Baird, A. J., and Belyea, L. R.: The DigiBog peatland development model 2: ecohydrological simulations in 2D, Ecohydrology, 5, 256-268, https://doi.org/10.1002/eco.229, 2012.

Morris, P. J., Baird, A. J., and Belyea, L. R.: The role of hydrological transience in peatland pattern formation, Earth Surf. Dynam., 1, 29-43, https://doi.org/10.5194/esurf-1-29-2013, 2013.

735 Morris, P. J., Belyea, L. R., and Baird, A. J.: Ecohydrological feedbacks in peatland development: a theoretical modelling study, Journal of Ecology, 99, 1190-1201, https://doi.org/10.1111/j.1365-2745.2011.01842.x, 2011.

Morris, P. J., Baird, A. J., Young, D. M., and Swindles, G. T.: Untangling climate signals from autogenic changes in long-term peatland development, Geophysical Research Letters, 42, 10,788-710,797, https://doi.org/10.1002/2015GL066824, 2015.

740 Munir, T. M., Perkins, M., Kaing, E., and Strack, M.: Carbon dioxide flux and net primary production of a boreal treed bog: Responses to warming and water-table-lowering simulations of climate change, Biogeosciences, 12, 1091-1111, https://doi.org/10.5194/bg-12-1091-2015, 2015.

O'Kelly, B. C.: Measurement, interpretation and recommended use of laboratory strength properties of fibrous peat, Geotechnical Research, 4, 136-171, https://doi.org/10.1680/jgere.17.00006, 2017.

745 Peltoniemi, K., Laiho, R., Juottonen, H., Bodrossy, L., Kell, D. K., Minkkinen, K., Mäkiranta, P., Mehtätalo, L., Penttilä, T., Siljanen, H. M. P., Tuittila, E.-S., Tuomivirta, T., and Fritze, H.: Responses of methanogenic and methanotrophic communities to warming in varying moisture regimes of two boreal fens, Soil Biology and Biochemistry, 97, 144-156, https://doi.org/10.1016/j.soilbio.2016.03.007, 2016.

Phillips, P. J. and Wheeler, M. F.: A coupling of mixed and continuous Galerkin finite element methods for poroelasticity I: 750 the continuous in time case, Computational Geosciences, 11, 131-144, https://doi.org/10.1007/s10596-007-9045-y, 2007.

Potvin, L. R., Kane, E. S., Chimner, R. A., Kolka, R. K., and Lilleskov, E. A.: Effects of water table position and plant functional group on plant community, aboveground production, and peat properties in a peatland mesocosm experiment (PEATcosm), Plant and Soil, 387, 277-294, https://doi.org/10.1007/s11104-014-2301-8, 2015.

755 Price, J. S.: Role and character of seasonal peat soil deformation on the hydrology of undisturbed and cutover peatlands, Water Resources Research, 39, https://doi.org/10.1029/2002WR001302, 2003.

Price, J. S. and Schlotzhauer, S. M.: Importance of shrinkage and compression in determining water storage changes in peat: the case of a mined peatland, Hydrological Processes, 13, 2591-2601, https://doi.org/10.1002/(SICI)1099-1085(199911)13:16<2591::AID-HYP933>3.0.CO;2-E, 1999.

760 Price, J. S., Cagampan, J., and Kellner, E.: Assessment of peat compressibility: is there an easy way?, Hydrological Processes, 19, 3469-3475, https://doi.org/10.1002/hyp.6068, 2005.

Quinton, W. L., Gray, D. M., and Marsh, P.: Subsurface drainage from hummock-covered hillslopes in the Arctic tundra, Journal of Hydrology, 237, 113-125, https://doi.org/10.1016/S0022-1694(00)00304-8, 2000.

Quinton, W. L., Hayashi, M., and Carey, S. K.: Peat hydraulic conductivity in cold regions and its relation to pore size and 765 geometry, Hydrological Processes, 22, 2829-2837, https://doi.org/10.1002/hyp.7027, 2008.

Reeve, A. S., Glaser, P. H., and Rosenberry, D. O.: Seasonal changes in peatland surface elevation recorded at GPS stations in the Red Lake Peatlands, northern Minnesota, USA, Journal of Geophysical Research: Biogeosciences, 118, 1616-1626, https://doi.org/10.1002/2013JG002404, 2013.

Reeve, A. S., Evensen, R., Glaser, P. H., Siegel, D. I., and Rosenberry, D.: Flow path oscillations in transient ground-water 770 simulations of large peatland systems, Journal of Hydrology, 316, 313-324, https://doi.org/10.1016/j.jhydrol.2005.05.005, 2006.

Regan, S., Flynn, R., Gill, L., Naughton, O., and Johnston, P.: Impacts of Groundwater Drainage on Peatland Subsidence and Its Ecological Implications on an Atlantic Raised Bog, Water Resources Research, 55, 6153-6168, https://doi.org/10.1029/2019WR024937, 2019.

775 Rydin, H. and Jeglum, J.: The Biology of Peatlands, Oxford University Press, Oxford, 2006.

Shewchuk, J. R.: Delaunay refinement algorithms for triangular mesh generation, Computational Geometry, 22, 21-74, https://doi.org/10.1016/S0925-7721(01)00047-5, 2002.

Swinnen, W., Broothaerts, N., and Verstraeten, G.: Modelling long-term blanket peatland development in eastern Scotland, Biogeosciences, 16, 3977-3996, https://doi.org/10.5194/bg-16-3977-2019, 2019.

780 Tarvainen, O., Hökkä, H., Kumpula, J., and Tolvanen, A.: Bringing back reindeer pastures in cutaway peatlands, Restoration Ecology, 30, e13661, https://doi.org/10.1111/rec.13661, 2022.

Terzaghi, K.: Theoretical soil mechanics, John Wiley & Sons, Inc, New York, 1943.

Tezduyar, T. E.: Finite element methods for flow problems with moving boundaries and interfaces, Archives of Computational Methods in Engineering, 8, 83-130, https://doi.org/10.1007/BF02897870, 2001.

785 Tuukkanen, T., Marttila, H., and Kløve, B.: Predicting organic matter, nitrogen, and phosphorus concentrations in runoff from peat extraction sites using partial least squares regression, Water Resources Research, 53, 5860-5876, https://doi.org/10.1002/2017WR020557, 2017.

Waddington, J. M., Kellner, E., Strack, M., and Price, J. S.: Differential peat deformation, compressibility, and water storage between peatland microforms: Implications for ecosystem function and development, Water Resources Research, 790 46, https://doi.org/10.1029/2009WR008802, 2010.

Wang, H. F.: Theory of linear poroelasticity with applications to geomechanics and hydrology, Princeton University Press, Princeton, NJ, USA, 2000.

Warburton, J., Higgitt, D., and Mills, A.: Anatomy of a Pennine peat slide, Northern England, Earth Surface Processes and Landforms, 28, 457-473, https://doi.org/10.1002/esp.452, 2003.

795 Whittington, P., Strack, M., Haarlem, R. v., Kaufman, S., P. Stoesser, Maltez, J., Price, J. S., and Stone, M.: The influence of peat volume change and vegetation on the hydrology of a kettle-hole wetland in Southern Ontario, Canada, Mires and Peat, 2, 2007.

Whittington, P. N. and Price, J. S.: The effects of water table draw-down (as a surrogate for climate change) on the hydrology of a fen peatland, Canada, Hydrological Processes, 20, 3589-3600, https://doi.org/10.1002/hyp.6376, 2006.

Winston, R. B.: Models of the geomorphology, hydrology, and development of domed peat bodies, GSA Bulletin, 106, 1594-1604, https://doi.org/10.1130/0016-7606(1994)106<1594:Motgha>2.3.Co;2, 1994.

Winter, T. C.: The concept of hydrologic landscapes, Journal of the American Water Resources Association, 37, 335-349, https://doi.org/10.1111/j.1752-1688.2001.tb00973.x, 2001.

805 Young, D. M., Baird, A. J., Gallego-Sala, A. V., and Loisel, J.: A cautionary tale about using the apparent carbon accumulation rate (aCAR) obtained from peat cores, Scientific Reports, 11, 9547, https://doi.org/10.1038/s41598-021-88766-8, 2021.

Young, D. M., Baird, A. J., Charman, D. J., Evans, C. D., Gallego-Sala, A. V., Gill, P. J., Hughes, P. D. M., Morris, P. J., and Swindles, G. T.: Misinterpreting carbon accumulation rates in records from near-surface peat, Scientific 810 Reports, 9, 17939, https://doi.org/10.1038/s41598-019-53879-8, 2019.

Yu, Z., Beilman, D. W., and Jones, M. C.: Sensitivity of Northern Peatland Carbon Dynamics to Holocene Climate Change, in: Carbon Cycling in Northern Peatlands, 55-69, https://doi.org/10.1029/2008GM000822, 2009.

Yu, Z., Loisel, J., Brosseau, D. P., Beilman, D. W., and Hunt, S. J.: Global peatland dynamics since the Last Glacial Maximum, Geophysical Research Letters, 37, https://doi.org/10.1029/2010GL043584, 2010.

815 Zhu, J., Wang, Y., Wang, Y., Mao, Z., and Langendoen, E. J.: How does root biodegradation after plant felling change root reinforcement to soil?, Plant and Soil, 446, 211-227, https://doi.org/10.1007/s11104-019-04345-x, 2020.

Zhu, X., Wang, Y., Zan, J., and Li, C.: Application of fractal theory in generation and refinement of finite element mesh, Applied Mathematics and Computation, 175, 1039-1045, https://doi.org/10.1016/j.amc.2005.08.017, 2006.